博士論文

An Optimal Design on Sustainable Hybrid Energy Systems by Multiobjective Functions for Shrimp Aquaculture Industry (エビ養殖業のための持続可能なハイブリッドエネルギーシステムに関する多目的評価関数に基づく最適設計)

令和 2 年 06 月 01 日提出

指導教員　松橋　隆治教授

東京大学大学院工学系研究科

電気系工学専攻

37-177267

グエン　ニュット　ティエン

Keywords

Onsite pure oxygen, electrolyzer, renewable energy, fuel cell, by-product hydrogen, elitist genetic optimization algorithm, aeration, shrimp farm.

Abstract

The shrimp aquaculture industry has been rising significantly, not only around the world but also in Vietnam. The shrimp farming in the Mekong Delta, Vietnam, makes a substantial contribution to the national economy via exporting to foreign countries. However, the energy consumption for the shrimp farming industry has continued rising considerably in recent years due to the expansion of shrimp production to meet food demand. Most of the energy demand at shrimp farms is consumed by the aeration system, which utilizes electrical motors to drive aerators for maintaining suitable dissolved oxygen in ponds continuously for improving water quality and promoting shrimp growth. Moreover, the intensive energy consumption from electric motors for aeration and pumping systems leads to high operation costs and associated greenhouse gas emission from using conventional power resources. Although many improvements have been made for the design and operation of aerators and even renewable energy resources have been applied, the traditional aeration system inherently consumes high power with low oxygen transfer from the air. This dissertation, therefore, proposes an optimal design on a sustainable hybrid energy system by multiobjective functions for the shrimp aquaculture industry.

The proposed system harnesses renewable energy resources to power the electrolyzer to produce pure oxygen in situ for oxygenation according to the changes of species under culture. In addition, the by-product hydrogen from the electrolysis process could be used for either commercial purposes or backup power. The mathematical models of the system were developed for simulation and optimization to assess the performance of the system regarding technical, economic, and environmental aspects as multiobjective functions in autonomous mode as well as on-grid mode. Besides, the optimal results and their sensitivity analysis showed that the sustainable hybrid energy system connecting to the national grid in which the by-product hydrogen is primarily either sold for commercial purposes or used for backup power could bring significant benefits for farmers thanks to a notable reduction in the annualized cost the system as well as CO_2 emission in comparison with the conventional system run by common paddlewheel aerators.

Declaration

I declare that the dissertation, which is entitled “An Optimal Design on Sustainable Hybrid Energy Systems by Multiobjective Functions for Shrimp Aquaculture Industry” and submitted in partial fulfillment for the award of Doctor of Philosophy in the Department of Electrical Engineering and Information Systems to the University of Tokyo, is the result carried out by my own work and effort under the guidance of Prof. Ryuji Matsuhashi.

The work is original and has not been submitted for any degree or diploma to any other university.

Tokyo, June 2020.

Table of Contents

Keywords ii
Abstract iii
Declaration iv
Table of Contents v
Nomenclature vii
List of Acronyms xv
List of Figures xvi
List of Tables xvii
Acknowledgments xviii

1. INTRODUCTION 1

1.1 General 1
1.2 Literature Review 2
1.3 Dissertation Objectives and Contributions 4
1.4 Dissertation Organisation 5

2. AERATION SYSTEMS FOR SHRIMP FARMS 6

2.1 Shrimp Farm Context in the Mekong Delta 6
2.1.1 Levels of Intensification in Shrimp Aquaculture 6
2.1.2 Economic and Environmental Essence of Shrimp Aquaculture 7
2.2 Importance of Water Quality and Dissolved Oxygen 8
2.3 Factors Affecting Dissolved Oxygen Concentration 9
2.4 Current State of the Art in Aquaculture Aeration 9
2.4.1 History of Aeration 9
2.4.2 Principles of Aeration 10
2.4.3 Oxygen Transfer Rate and Efficiency of Mechanical Aerators 11
2.4.4 Types of Aerators 13

3. SUSTAINABLE HYBRID ENERGY SYSTEMS FOR SHRIMP FARMS 17

3.1 Potential of Renewable Energy Resources in the Mekong Delta 17
3.2 Proposed System Configuration 17
3.3 System Operation 18
3.3.1 Hydrogen Used for Commercial Purposes 20
3.3.2 Hydrogen Used for Backup Power 21
3.4 Power Management Strategy 22
3.4.1 Hydrogen Used for Commercial Purposes 22
3.4.2 Hydrogen Used for Backup Power 24

4. OPTIMAL DESIGN ON SUSTAINABLE HYBRID ENERGY SYSTEMS BY MULTIOBJECTIVE FUNCTIONS 27

4.1 Power Load Model (PL) 27
4.1.1 Dissolved Oxygen Model (DO) 27
4.1.2 Power Capacity of Electrolyzer 29
4.1.3 Power Capacity of Mechanical Aerator 30
4.2 Solar Photovoltaic Model (PV) 31
4.3 Wind Turbine Model (WT) 32

4.4 Battery Bank Model (BB) 33
4.5 Fuel Cell Model (FC) 33
4.6 Hydrogen Tank Model (HT) 33
4.7 Diesel Generator Model (DG) 34
4.8 Objective Functions 34
4.8.1 Annualized Cost of System (ACS) 34
4.8.2 Loss of Power Supply Percentage (LPSP) 36
4.8.3 Carbon Dioxide Emission (EMI) 37
4.9 Multiobjective Optimization for Sustainable Hybrid Energy Systems 37
4.9.1 Constraints 37
4.9.2 Implementation of Non-dominated Sorted Genetic Algorithm (NSGA-II) 39
4.10 Sensitivity Analysis for Sustainable Hybrid Energy Systems 41
4.10.1 The External Uncertainty Models 41
4.10.2 Sensitivity Analysis by Monte Carlo Simulation 42
5. ANALYSIS OF SUSTAINABLE HYBRID ENERGY SYSTEMS FOR SHRIMP FARMS 45
5.1 Case Study 45
5.1.1 Case Data Introduction 45
5.1.2 Parameter Settings 48
5.2 Hydrogen Used for Commercial Purposes 49
5.2.1 Scenarios for Simulation Optimization 49
5.2.2 Optimization Results in Stand-Alone Mode for Scenario S1 50
5.2.3 Optimization Results in Stand-Alone Mode for Scenario S2 51
5.2.4 Optimization Results in Stand-Alone Mode for Scenario S3 53
5.2.5 Optimization Results in Grid-Connected Mode 54
5.3 Hydrogen Used for Backup Power 55
5.3.1 Optimization Results in Stand-Alone Mode 55
5.3.2 Optimization Results in Grid-Connected Mode 58
5.4 Potential Carbon Tax and Sensitivity Analysis 60
5.4.1 Potential Carbon Tax Analysis 60
5.4.2 Sensitivity of Deterministic Solutions 61
6. CONCLUSION AND FUTURE WORKS 63
6.1 Conclusion 63
6.2 Future works 64
APPENDICES 66
BIBLIOGRAPHY 68
RESEARCH ACHIEVEMENTS 76
Oral Presentations 76
Publications 76

Nomenclature

10^{-3}	Converting factor from grams to kilograms
A	Membrane-electrode-assembly area
AAE	Actual aeration efficiency of aerator
A_{int}	Area of the interface where the transfer occurs
A_{PV}	Area of PV module
c_1	Intercept coefficient of fuel consumption curve
c_2	Slope of fuel consumption curve
c_{gp}	Purchasing electricity price
c_{gs}	Selling electricity price
c_{hs}	Selling price of hydrogen
$Chla$	Concentration of chlorophyll-a
$CRF(i,N)$	Capital recovery factor
C_{ACC}	Annualized cost of components in the system
C_{CAP}	Capital cost
C_{DTB}	Total depreciation tax benefit
C_{GP}	Total cost of purchasing electricity
C_{GS}	Total cost of selling electricity
$C_{H_2}(t)$	States of hydrogen mass in storage tank
$C_{H_2}^{\max}$	Maximum level of hydrogen
$C_{H_2}^{\min}$	Minimum level of hydrogen
C_{HS}	Total cost of selling surplus hydrogen

C_m	Measured concentration of DO in water pond
C_{MAI}	Total maintenance cost
C_{NPC}	Net present cost
C_p	Initial concentration in pond water
C_{REP}	Total replacement cost
C_s	DO concentration at saturation
C_s^{20}	Concentration of DO at saturation and 20 °C
C_{SV}	Total salvage value
C_t	Instantaneous DO concentration
dC_{O_2}/dt	Concentration gradient of oxygen
dDO/dt	Changing rate of DO level
dm_{O_2}/dt	Mass transfer rate of oxygen
DTB	Annual depreciation tax benefit
D_m	Molecular diffusion constant of oxygen
E_{BB}	Battery bank capacity
$E_{BB}^{\max}$	Maximum value of battery capacity.
e_{DF}	Diesel fuel emission factor
e_{grid}	Grid emission factor
E_{O_2}	Oxygen exchange rate
F	Faraday's number
FC_{DG}	Fuel consumption rate of diesel generator
F_{eff}	Correction factor considering the high consumption
G	Global solar radiation on tilted surface

G_b	Beam component of global solar radiation
G_d	Diffuse component of global solar radiation
G_d^h	Diffuse horizontal radiation
G_g^h	Global horizontal radiation
G_r	Reflected component of global solar radiation
h	Hub height
h_{ref}	Reference height
i	Interest rate
I_{ELZ}	Operating current of electrolyzer
J	Current density
K_L	Oxygen transfer coefficient from wind
$K_L a_{20}$	Oxygen-transfer coefficient at 20 °C
$K_L a_{T_w}$	Oxygen-transfer coefficient
l_c	Lifetime of replaced components
MAI	Annual maintenance cost
$m_{H_2}^{cons}$	Hourly fuel consumption of FC
$m_{H_2}^{dumped}$	Surplus hydrogen
$m_{H_2}^{prod}$	Hydrogen mass flow produced from electrolyzer hourly
m_{HT}	Mass of HT
$m_{HT}^{\max}$	Mass of HT
m_j	Total number of pixels in the investigated area
m_{shrimp}	Wet body weight of shrimp
n	n-th year of the project

N	Project lifetime
N_c	Number of cells in an electrolyzer's stack
n_{H_2}	Number of electrons transferred hydrogen molecule
n_i	Site use suitability category number
N_{samp}	Number of discrete samples
OD	Oxygen deficit
OD_{10}	Oxygen deficit at 10% saturation
OD_{70}	Oxygen deficit at 70% saturation
PF_j	Packing factor
P_{ch}	Charging power
$P_{ch}^{\max}$	Maximum charging power of battery
P_{CP}	Capacity potential
P_d	Dumped power
P_{DG}	Output power of diesel generator
P_{DG}^{rated}	Rated power of diesel generator
P_{dis}	Discharging power
$P_{dis}^{\max}$	Maximum discharging power of battery
$P_{eff}^{\max}$	Power of maximum efficiency
P_{ELZ}	Power required by electrolyzer
P_{FC}	Output power of fuel cell
$P_{FC}^{\max}$	Maximum value of FC capacity
P_{FC}^{rated}	Capacity of fuel cell
P_{gen}	Power generated from renewable resources

P_{gp}	Power purchased from grid
P_{gs}	Power sold to national grid
P_{im}	Imbalance power
P_{load}	Power load demand
P_{MA}	Power applied to aerator
P_{O_2}	Photosynthesis production
P_{PV}	Output power of PV system
$P_{PV}^{\max}$	Maximum value of PV capacity
P_{PV}^{peak}	PV peak capacity
P_{PV}^{unit}	Power per unit area of PV array
P_{total}	Generated power from available resources
P_{unmet}	Unmet load at each hour
P_{WT}	Power produced by WT system
$P_{WT}^{\max}$	Maximum value of WT capacity
P_{WT}^{rated}	Rated power of WT
Q_{H_2}	Hydrogen gas flow rate
Q_{O_2}	Oxygen gas flow rate
r	r-th replacement
R	Total number of replacements
REP	Investment cost of replaced component
R_{O_2}	Total respiration of organisms
R_S	Broadband solar radiation
$R_{sediment}$	Sediment respiration rate

$R_{species}$	Respiration rate of species under culture
R_{water}	Water respiration rate
S	Salinity
SAE	Standard aeration efficiency
SF_i	Suitable fraction of site utilization type
$SOC(t)$	States of charge of battery bank
$SOC_{\max}$	Upper limit of the battery bank
$SOC_{\min}$	Lower limit of the battery bank
$SOTR$	Standard oxygen-transfer rate
St_{shrimp}	Stocking density of shrimp
SV	Salvage value
S_{ij}	Area of site use type
S_{O_2}	Percentage saturation
T	Number of hours in a year
TOD	Total oxygen demand
tr	Tax rate
t_{10}	Time when DO reaches 10% saturation
t_{70}	Time when DO reaches 70% saturation
T_{NOC}	Nominal operating cell temperature
T_{STC}	STC temperature
T_W	Water temperature
U	Supplied voltage
U_c	Cell's actual voltage
V_{pond}	Pond volume

v	Wind speed
v_i	Cut-in wind speed
v_o	Cut-out wind speed
v_r	Rated wind speed
v_{ref}	Measured wind speed at reference height
z_0	Surface roughness length
z_1	Control volume thickness affected by re-aeration
α	Ratio of mass-oxygen transfer coefficient between pond water and clean water basis
α_{FC}	Coefficient of hydrogen consumption curve
α_j	Dimensionless re-aeration adjustment coefficient
α_{par}	Ratio of PAR to broadband solar radiation
α_s	Solar altitude
β	Ratio of DO saturation concentration of pond water to tap water
β_{FC}	Coefficient of hydrogen consumption curve
β_t	Tilt angle
γ_a	Azimuth angle
σ_{BB}	Hourly self-discharge rate of battery
σ^2	Standard deviation
η_b	Gearbox/bearing efficiency
η_{BB}	Efficiency of battery bank
η_g	Generator efficiency
η_F	Faradic efficiency
η_{HT}	Storage efficiency of hydrogen tank

η_{inv}	Inverter efficiency
η_{PV}^{STC}	Module efficiency at standard test condition
η_{WT}	Efficiency of WT system
η_{μ}	Oxygen absorption efficiency generated by microbubble system
θ	Angle of incidence
$\theta_j(t)$	Uncertain parameters
μ	Annual mean
μ_{PV}	Temperature coefficient of output power
$\mathcal{N}$	Gaussian PDF
ρ_g	Ground reflectance
$\varphi_j(t)$	Time-dependent phenomena

List of Acronyms

ACS	Annualized Cost of System
BB	Battery Bank
DG	Diesel Generator
DO	Dissolved Oxygen
EMI	Emission
FC	Fuel Cell
HT	Hydrogen Tank
LPSP	Loss of Power Supply Percentage
PAR	Photosynthetically Active solar Radiation
PDF	Probabilistic Distribution Function
PL	Power Load
PV	Photovoltaic
STC	Standard Test Condition
WT	Wind Turbine

List of Figures

Figure 2.1 Diffused air aeration system [19]. 13
Figure 2.2 Propeller-aspirator pump [19]. 14
Figure 2.3 Vertical pump sprayer [19]. 15
Figure 2.4 Paddlewheel aerators [19]. 16
Figure 3.1 Sustainable hybrid energy system for aquaculture farms. 18
Figure 3.2 Sustainable hybrid energy system for aquaculture farms when hydrogen is sold to the fertilizer plant. 20
Figure 3.3 Sustainable hybrid energy system for aquaculture farms when hydrogen is used for backup power. 21
Figure 3.4 Flowchart of power management strategy when hydrogen is used for commercial purposes. 23
Figure 3.5 Flowchart of power management strategy when hydrogen is used for backup power. 25
Figure 4.1 Flowchart of NSGA-II for optimization under multiobjective functions. 40
Figure 4.2 Framework of scenario development by Monte Carlo simulation for sensitivity analysis. 43
Figure 5.1 Ponds at the investigated shrimp farm. 45
Figure 5.2 Annual solar irradiance (a), air temperature (b), and wind speed at 10 m height (c). 46
Figure 5.3 Hourly oxygen rate by photosynthesis process and respiration demand. 47
Figure 5.4 Hourly oxygen requirement and power demand at the shrimp farm. 48
Figure 5.5 Pareto front for scenario S1. 50
Figure 5.6 The relationship between PV and battery capacity with emission. 51
Figure 5.7 Pareto front for scenario S2. 52
Figure 5.8 The relationship between wind turbine and battery capacity with emission. 52
Figure 5.9 Pareto front for scenario S3. 53
Figure 5.10 Pareto front for on-grid mode. 54
Figure 5.11 Pareto fronts in stand-alone mode. 56
Figure 5.12 The relationship between the capacity of PV and WT with LPSP. 57
Figure 5.13 The relationship between FC capacity and LPSP with ACS. 58
Figure 5.14 Pareto front for on-grid operation mode. 59
Figure 5.15 PDFs of the results of ACS (a) and EMI (b) for on-grid operation mode. 61
Figure 5.16 PDFs of the results of ACS (a) and EMI (b) for Sol 2. 61

List of Tables

Table 2.1 Characteristics of shrimp culture systems 6
Table 5.1 Biophysical characteristics of grow-out ponds 47
Table 5.2 Parameter settings for simulation optimization 49
Table 5.3 Summary of simulated scenarios 50
Table 5.4 Optimization results corresponding with the minimum annualized cost of system for each scenario. 54
Table 5.5 Comparison between scenario S3, on-grid mode and conventional aeration system. 55
Table 5.6 Characteristics of two solutions of interest and conventional aeration system 59
Table 5.7 Potential carbon tax of scenarios compared to the CAS 60
Table 5.8 Results of sensitivity analysis for on-grid mode and Sol 2 62

Acknowledgments

First and foremost, I would sincerely like to express my deepest gratitude to my supervisor, Prof. Ryuji Matsuhashi, for his invaluable guidance, precious advice, and encouragement throughout my graduate studies. All of my works in this dissertation might not be achieved without his support.

I wish to extend my hearty thanks to the Can Tho University Improvement Project VN14-P6 through the Japanese Official Development Assistance (ODA) Loan. Funding and financial support from the project are gratefully acknowledged.

Moreover, I want to thank the Department of Electrical Engineering and Information Systems of the University of Tokyo for giving me the opportunity to study and research during my academic endeavors in graduate school.

Besides, I am genuinely grateful to my family for supporting me during a long period of studying and researching.

I would also like to thank my friends as well as my colleagues for their encouragement and companionship.

Last but not least, I would like to express my appreciation from the bottom of my heart to my wife, Chau, for her love and encouragement. Thanks for her understanding, staying by my side, and taking care of our lovely daughter.

Nguyen Nhut Tien

June 2020

1. Introduction

1.1 General

Aquaculture around the world has experienced considerable growth during the last decades. Global aquaculture production has been continuing to rise significantly to meet the food demand of the world, being estimated to witness an increase of around 4% in 2019 [1]. In addition, the production of the aquaculture sector is mainly located in Asia, which accounts for 89% of world aquaculture production [2]. The aquaculture sector is a vital source of food security, protein, and economic driver for the world today. Among common seafood products such as salmon, pangasius, tuna, tilapia, etc., shrimp is considered to be one of the commercial commodities worldwide [3].

Shrimp farming has begun since the second half of the 20th century, which currently constitutes about 30% of global shrimp production and 40% of shrimp export [4]. Furthermore, thanks to the advanced technology, the farmed shrimp production around the globe reached about four million tons in 2018, which is contributed from Asia, such as China, India, Vietnam, Indonesia, Thailand, Philippines, Bangladesh, and Malaysia [5].

Vietnam is one of the major shrimp producers in the world, being ranked second in the global exporters of shrimp in 2017 and 2018, and the production continues to increase in 2019 [5]. Moreover, shrimp production in the Mekong Delta, Vietnam, makes up 75%, with the total shrimp farming area about 90% [6]. The shrimp production systems in Vietnam are mainly classified into small-scale producers and processing companies with the rearing method being quickly shifted from extensive models having low density to semi-intensive, intensive, and ultra-intensive models with high density. However, the fast growth of shrimp aquaculture production has been accomplished in part through high intensity, which acquires dramatically high energy demand.

Although the shrimp farming industry not only supplies food but also contributes income to farmers and their country, shrimp aquaculture is associated with environmental issues and energy security. The main cause of ecological problems is the salination of local land [7] and the pollution of water resources [8]. Besides, the

energy demand is one of the major challenges of the shrimp industry because most of the energy is consumed by water pumps and pond aerators, which run 24h per day [9]. Electric aerators constitute about 80% of farm energy demand while pumping water accounts for 10%, leaving other usages at 10% [10]. Furthermore, the energy efficiency of marine shrimp aquaculture systems, which is the ratio between the food protein-energy output and industrial energy input, is very low among the significant aquaculture systems [9]. The cause of inefficient systems is the high electrical consumption of machines and aerators that have a typical efficiency of about 90% [11].

One of the big problems in shrimp farming is the expense of maintaining the quality of water. In fact, the concentration of dissolved oxygen (DO) in cultivating ponds is one of the critical parameters to ensure the health and survivability of species under culture. Shrimps reared in ponds, which are quite different from species living in rivers and sea, require a high amount of DO in the pond, especially in the intensive aquaculture system. The water in ponds with high DO concentration is considered high quality, which is necessary for the success and development of shrimp farming [12], [13]. As a result, aeration systems are employed to improve oxygen content [11], [14], [15], [16].

1.2 Literature Review

Mechanical aerators are the most popular means used not only to supplement DO to aquaculture ponds but also to circulate oxygen availability in the water over the bottom of the pond. Aeration systems make it possible for higher stocking and feed input. Furthermore, dissolved oxygen, which indicates the water quality, plays a vital role in aquaculture ponds; hence, it is necessary to understand elaborately factors that might cause a decrease in DO concentration to prevent low concentration in ponds [17]. In semi-intensive shrimp aquaculture, aeration devices are utilized in emergencies when the level of DO in ponds drops below the acceptable concentration of 3 mg/L [18]. In intensive and ultra-intensive aquaculture, aerators are usually operated at night more frequently than in daytime to avoid low levels of DO, which might cause shrimp stress or even death.

Aquaculture aerators are modified from those applied in wastewater treatment systems; therefore, both of them share the same principles and design features [4]. In general, there are three popular types of aerators, such as splasher, bubbler, and pure oxygen system [19]. Bubbler and splasher aerators are driven by motors and pumps

powered by the national network or diesel fuel in remote areas to increase the oxygen transfer rate between the air and the water in the pond. The pure oxygen contact system improves DO concentration by releasing oxygen bubbles into the water. The two common types of aerators utilized for aeration systems are paddlewheel and propeller-aspirator-pump aerators since their oxygen transfer and water circulation are efficient [20].

During a 100-day production of marine shrimp farming, aerators are often run continuously during a day [9] even when the DO level in the pond is saturated, resulting in off-gassing DO, wasted energy, and high operation costs [11]. Thus, the aeration system should be designed carefully and operated optimally to improve energy management [21]. In order to maintain suitable DO and reduce power consumption, some investigations focusing on controlling aerators have been considered. For instance, reference [22] shows the benefit of reducing energy consumption when aerators are controlled in intermittent mode. Furthermore, the automatic control proposed in [23] and intelligent control described in [24], [25], and [26] also effectively decrease the energy requirement of aeration technologies.

Besides, the configurations of mechanical aerators have been modified to improve their aeration efficiency and energy cost [27]. In addition, a study on different configurations of impeller aerators developed by [28] tried to achieve the highest aeration efficiency. On the one hand, the optimal rotation speed is taken into account to evaluate the nexus between energy requirement and oxygen transfer for widely-used surface aerators such as paddlewheel aerators in [16], [29] and spiral aerators in [30]. On the other hand, the new generation of aerators, namely impeller in [31], centrifugal water stirrer in [32], and new tube aeration device in [33], have been applied in aquaculture and enhanced oxygenation energy-saving technology with high performance.

Moreover, to achieve energy savings and emission reduction, renewable energy resources have been being harnessed for the aquaculture industry as these energy sources are estimated to increase significantly in the future [34]. Photovoltaic energy is supplied to control the oxygen levels in fish tanks in [35]. Floating and floating-tracking PV systems are employed for shrimp farms in Thailand, producing energy self-sufficiency with high reliability and better competitiveness by limiting energy storage system [36]. Furthermore, the combination between PV and solar-thermal panels is

utilized to provide not only electric load but also thermal load for the fish farm [37]. A solar-thermal aeration system in [38] is introduced to circulate oxygen to deeper layers of the pond for aquaculture in rural areas. Likewise, wind energy is solely employed for small-scale fish farms in developing countries [39] and for small-scale prawn farm in [40], or combined with a PV system in [41] to power the farm. Renewable energy is also employed not only for on-shore but also off-shore aquaculture with promising results [42], [43]. Besides, hydrogen and fuel cell technology have recently become popular and a great promising alternative resource [44]. The hydrogen, which can be stored in large volumes and generated into electricity by fuel cells, has dominated other storage technologies. Proton-exchange membrane fuel cells produce power from hydrogen for aeration system in stagnant ponds [45], [46]. Notably, the local biogas waste at a shrimp farm in the Mekong Delta, Vietnam, is used to generate hydrogen, which is produced by dry reforming methane for power generation [47].

Despite the improvements for aerators and the employment of green energy for aquaculture, demerits of conventional aeration systems are low aeration efficiency and high energy consumption due to atmospheric oxygenation, which accounts for 21%. Using pure oxygen instead of oxygen in the atmosphere for aeration system might reduce energy demand and raise yield; nevertheless, the operation cost of such a system is expensive due to extra transporting costs from suppliers to customers, which causes associated greenhouse gas emissions. Although pure oxygen has been broadly applied in such industrial processes as combustion, semiconductor production, and wastewater treatment because of improving system efficiency [48], there are few works about utilizing pure oxygen from water electrolysis for aeration system in aquaculture [49]. Apart from that, there is no study in which an aeration system energized by renewable energy is proposed to produce onsite oxygen and employs by-product hydrogen for different applications.

1.3 Dissertation Objectives and Contributions

This dissertation proposes an optimal design on sustainable hybrid energy systems for the shrimp aquaculture industry, which utilizes renewable energy to provide pure oxygen onsite from the electrolysis process for oxygenation according to the DO demand of shrimp. Moreover, the self-product hydrogen through water electrolysis is sold to local fertilizer plants or stored for backup power. The whole system is optimized by multiobjective functions, such as the annualized cost of the

system, loss of power supply percentage, and carbon dioxide emission in different operation modes corresponding to various system configurations. Consequently, the sensitivity analysis of optimal solutions from the proposed system is carried out by Monte Carlo simulation to make comparisons with a conventional aeration system run by widely-used paddlewheel aerators in terms of the annualized cost of the system and the emission of CO_2.

The main contributions of this work include the following:

- A conceptual design on sustainable hybrid energy systems for shrimp farms is implemented for aeration system in which green technology is applied to produce pure oxygen onsite according to DO demand of shrimps, leading to higher yield and energy saving. Besides, the by-product hydrogen is used for different applications.
- The power load model is developed to calculate the rated capacity of the electrolyzer according to the change of DO concentration in the pond.
- Mathematical models are developed in the Matlab environment for optimization simulation according to multiobjective functions.
- Potential carbon tax and sensitivity analysis by Monte Carlo simulation are carried out to evaluate the optimal outcomes.
- The optimal design of the energy system helps farmers save operation costs and reduce CO_2. Moreover, this work is useful guidelines to instruct optimum design and operation for aquaculture farms.

1.4 Dissertation Organisation

The structure of the dissertation is organized into six sections in detail below.

Section 2 presents aeration systems for shrimp farms.

Section 3 illustrated the proposed, sustainable hybrid energy system for shrimp farms.

Section 4 describes the optimal design of hybrid energy systems by multiobjective functions.

Section 5 discusses the analysis of sustainable hybrid energy systems for shrimp farms.

Section 6 gives the summary and scope for the future work of this dissertation.

2. Aeration Systems for Shrimp Farms

2.1 Shrimp Farm Context in the Mekong Delta

Shrimp aquaculture in Vietnam has begun since the 1990s with cultivating area and shrimp production growing from 230,000 ha and 56,000 tonnes in 1991 [50] to 706,000 ha and 701,000 tonnes in 2017 [51], respectively. The Mekong Delta has the largest shrimp farming area, which substitutes about 90% of the total area, contributing 75% to the product of the country [6]. Besides, Vietnam is considered the leading exporter of valued-added shrimp to the United States of America, Japan, and the EU28, with an export value of 3.85 billion USD [51]. The systems of shrimp production in Vietnam include small-scale producers and processing companies. Small-scale households play a dominant role in total production [50] while the processing companies, which have their ponds for rearing with the maximum processing capacity of 20% [52].

2.1.1 Levels of Intensification in Shrimp Aquaculture

Shrimp culture systems are broadly categorized based on yield potentials and operating characteristics. The levels of intensification of shrimp culture are divided into four main categories, such as extensive, semi-intensive, intensive, and ultra-intensive [53]. Various characteristics, such as production level, stocking densities, aeration, and energy consumption, determining different categories of intensity, are illustrated in Table 2.1 [53],[54].

Table 2.1 Characteristics of shrimp culture systems

Characteristics	Production type			
	Extensive	Semi-intensive	Intensive	Ultra-intensive
Production (MT/ha/year)	0.1-0.3	0.5-2.5	5-15	30-150
Stocking rate (#/m^2/crop)	0.1-1	3-10	15-40	>100
Aeration	natural	water exchange	aerators	aerators
Potential energy demand (hp/ha)	0-2	2-5	15-20	>25

Among categories of intensity shown in Table 2.1, extensive ponds have the lowest stocking densities, which constitute less than one juvenile/m^2/crop. Consequently, the extensive systems produce low yields under 50 kg/ha/year from one or two crops in a year. The extensive culture relies not only on natural nutrients in the

pond but also on balanced biological and physical processes to ensure sufficient oxygen levels for shrimp without food supplements and human intervention. Stocking densities and yields can be increased by implementing different management actions for higher levels of intensification. As the intensification increases, such systems require a significant amount of supplemental and formulated feeds, water quality monitor, and utilization of mechanical aerators, especially for intensive and ultra-intensive systems. Higher intensity culture systems often coincide with high energy demand, which is consumed by water pumping and aeration. Energy capacity rises significantly with intensification ranging from 15 to 20 and more than 25 hp/ha for intensive and ultra-intensive systems, respectively.

2.1.2 Economic and Environmental Essence of Shrimp Aquaculture

The shrimp culture in Vietnam is mainly classified into small-scale producers and processing companies, with the modern culture systems being changed from extensive systems to intensive and ultra-intensive systems, which require supplementary technologies such as mechanical aerators.

Mechanical aerators are a powerful device to maintain water quality. Aerators operate at night more frequently than in the daytime; nonetheless, as shrimp culture intensifies, it is necessary to supply aeration 24 h/day. In addition, shrimps need more dissolved oxygen as they grow, resulting in an increase in aeration capacity, which requires high capital cost.

Although the benefits of mechanical aeration are not deniable, aeration systems consume a considerable amount of energy. The actual consumption of electrical energy is 1.26 times higher than the shaft power of aerators [55]. Furthermore, the electricity price for powering electrical motors, which drive the mechanical aerators, is high; nevertheless, aerators often run in an ad-hoc operation mode, leading to higher operational costs than required. The total production cost, however, might be reduced by restricting aerators' operation to necessary periods, especially in regions where electricity price is costly during the day. In other words, the use of aeration for shrimp culture should be taken into account to save energy costs because excessive aeration is wasteful, increasing additional expenses, such as maintenance costs and associated infrastructure [19]. Nonetheless, to ensure the safe dissolved oxygen for shrimp, the oxygenation supply from aeration, in reality, is higher than the oxygen

demand of cultured ponds [18] since there is no methodology to compute precisely the amount of required oxygen to maintain stable DO in the ponds [19].

Shrimp culture systems rely heavily on electrical energy, particularly aeration systems, which make up 80% of the total energy at the farm [10]. Such shrimp farms usually equip the aeration system with either mobile diesel or a gasoline generator to cope with temporary blackouts as the failure of electrical supply might cause a significant drop in dissolved oxygen in shrimp ponds. This situation becomes more dangerous for high-intensity culture or the growing state of shrimp, which is one of the main reasons leading to a high mortal rate of shrimp due to the low oxygen level [4]. Most of the power employed to operate aerators is derived from fossil fuel, which causes substantial financial and environmental impacts. It is well-documented that producing one tonne of prawn corresponds with about ten tonnes of CO_2 released from the stacks of coal-fired power plants [10]. Besides, the cost of using diesel fuel for driving electric motors of aeration systems is much higher than the electricity purchased from the national grid.

A sustainable energy system should be proposed based on these observations to aerate shrimp ponds, especially in the context of encouraging the development of high technology with energy-saving and sustainability for the shrimp industry in Vietnam.

2.2 Importance of Water Quality and Dissolved Oxygen

Water quality, which is determined by complex biological, chemical, and physical processes, plays a critical role in shrimp aquaculture [56]. Water quality includes many vital factors, which affect the shrimp culture, such as survival, growth, and yields. Understanding these factors might help farmers determine the potential of the water environment to improve water quality, to reduce stress on shrimp, to lower the susceptivity of shrimp to diseases, to produce high-quality products, to decrease the impacts of effluents on the environment, and procure higher profits.

The variables of water quality commonly monitored in shrimp ponds are water pH, temperature, salinity, dissolved oxygen, ammonia, plankton population, nitrite, hydrogen sulfide, and water clarity [57]. Among the water quality variables, dissolved oxygen is the most critical since it improves shrimp survival and enhances shrimp growth. In contrast, the deficiency in dissolved oxygen leads to slow growth and increases the vulnerability to diseases or even death due to hypoxia [19].

2.3 Factors Affecting Dissolved Oxygen Concentration

The natural budgets of oxygen are mainly derived from photosynthesis by phytoplankton and diffusion from the atmosphere. During daylight, a large amount of oxygen in the pond is produced by photosynthesis, which is higher than the respiration of the pond. This case leads to dissolved oxygen saturation when the pressure of oxygen in the water pond is equal to that in air. There are a lot of factors affecting oxygen saturation, as well as oxygen dynamics in the water pond.

The dissolved oxygen concentrations at saturation change according to temperature, salinity, and barometer pressure [11]. The solubility of oxygen in the water pond decreases as the temperature increases [11], which means that water with higher temperature has a lower level of dissolved oxygen at saturation than colder water. Moreover, the dissolved oxygen content decreases with the rise of salinity [11]. The cause of low oxygen solubility at saturation is the introduction of ionic salt, whose ions attract water molecules [58]. The barometric pressure has a small effect on the oxygen solubility in shrimp ponds [11]. Generally, it is necessary to sustain sufficient oxygen budgets for shrimp production due to many variables affecting dissolved oxygen in the water pond. The oxygen supplement for shrimp ponds is attained by aeration systems.

2.4 Current State of the Art in Aquaculture Aeration

2.4.1 History of Aeration

Food plays an important role in shrimp aquaculture; nevertheless, low concentrations of dissolved oxygen limit the shrimp production as the culture intensifies. The oxygen contents are improved through the use of mechanical aerators. Aeration for aquaculture is not new, but this technique has been applied and attracted lots of interest over the past many years.

The aeration system for shrimp aquaculture is modified from mechanical aeration of wastewater, which was utilized for research in the 1880s and 1890s, and then for municipal wastewater treatment systems from 1910 to 1930 [59]. In Asia, the paddlewheel aerators made in Taiwan were commonly used in pond aquaculture as early as the 1950s [19]. Electric small aerators with the power ranging from 0.25 to 2 hp are widely applied for smaller cultured ponds, especially Taiwanese aerators due to their high efficiency as well as affordable costs [16].

2.4.2 Principles of Aeration

The oxygen in the air accounts for 21%. Basically, the pressure in the atmosphere is greater than that in the water pond; hence, the oxygen in the air is driven into the water at the surface of the pond. This process ceases as the pressure in the air is equal to that in the water pond, leading to saturation of dissolved oxygen in the water. The oxygen content in shrimp ponds varies according to environmental factors in the pond, such as barometric pressure, temperature, and salinity [11]. Besides, the respiration rate of organisms and stocking densities in ponds also affect the concentration of DO [60].

Phytoplankton, which is constituted by ammonia and phosphate, is abundant in ponds, with photoautotrophs being capable of producing oxygen [4]. The level of DO in the daytime is higher than the saturated concentration because the amount of dissolved oxygen production is greater than the respiration rates of organisms in the cultured pond. On the contrary, the DO concentration decreases considerably at night or cloudy weather due to high respiration by shrimp crop, plankton, and benthos. Low levels of DO affect biophysical characteristics of shrimp, such as being gasped or suffering from stress, which leads to loss of appetite, vulnerability to diseases, low efficiency in using feeds, high mortal rate, and low yields [4].

The oxygen is produced at the surface layer of the water pond through the photosynthesis process. The oxygen content, therefore, decreases with the increase of the water depth and reaches the lowest value at the bottom of the pond [4]. Thus, shallow ponds are recommended for shrimp aquaculture [17] since shrimps live in the middle and the bottom layers of the pond [61]. The DO concentrations are maintained sufficiently for shrimp ponds by mixing high DO levels at the surface water with the water at deeper layers. Improving oxygen continuously in cultured ponds is critical to sustaining healthy life for shrimps, helping them grow faster, reducing diseases, increasing survival rate, and rising yields [4]. Thereby, oxygen-improving systems are necessary to be constructed for shrimp culture.

Mechanical aerators are employed to supply oxygen supplement for shrimp ponds, especially during the night or cloud cover, to compensate DO deficit due to respiration of organisms in the pond. Aerators are used in emergency cases under semi-intensive culture; nonetheless, they are operated every night or even continuously in case of intensive or ultra-intensive culture.

The mechanism of mechanical aerators aims at increasing contact of water with air and DO into the water. The DO concentration in shrimp ponds is improved as more oxygen in the atmosphere fills in the body of water. Mechanical aerators utilized in shrimp aquaculture include three common types, such as splasher, bubbler, and pure oxygen system [19].

2.4.3 Oxygen Transfer Rate and Efficiency of Mechanical Aerators

The oxygen transfer from the air into water happens at the gas-liquid interface via a gas film. Then the oxygen is transferred across the gas-liquid interface into the bulk water through the water film. It depends on the surface area of the interface and the concentration gradient of oxygen within the water. The relationship describing the rate of mass oxygen transfer is given by Fick's first law as:

$$\frac{dm_{O_2}}{dt} = D_m \cdot A_{int} \cdot \frac{dC_{O_2}}{dt} \tag{2.1}$$

where dm_{O_2}/dt is the mass transfer rate of oxygen (g/sec), D_m denotes the molecular diffusion constant of oxygen (cm^2/sec), A_{int} refers to the area of the interface where the transfer occurs (cm^2), dC_{O_2}/dt is the concentration gradient of oxygen (g/cm^4).

Mechanical aerators are employed to create a wider surface area and a high concentration gradient at the interface between the air and the water pond to increase oxygen transfer. Besides, the aerator increases the surface area by either breaking the water pond into small droplets lifted to the atmosphere or injecting air into the bulk water in the form of air bubbles [62].

The percentage saturation of dissolved oxygen concentration is expressed by:

$$S_{O_2} = \frac{C_m}{C_s} \cdot 100 \tag{2.2}$$

where S_{O_2} represents the percentage saturation, C_m refers to the measured concentration of DO in water pond (mg/L), C_s denotes DO concentration at saturation (mg/L).

Furthermore, the deficiency in oxygen is the difference between DO concentration at 100% saturation and measured DO in water, which is calculated as follows:

$$OD = C_s - C_m \tag{2.3}$$

where OD is oxygen deficit (mg/L).

The oxygen-transfer coefficient, which denotes concentrations of DO at 10% and 70% of saturation, is expressed as [62]:

$$K_L a_{T_W} = \frac{\ln OD_{10} - \ln OD_{70}}{t_{70} - t_{10}} \tag{2.4}$$

where $K_L a_{T_W}$ presents oxygen-transfer coefficient (h), OD_{10} and OD_{70} are oxygen deficit at 10% and 70% saturation (mg/L), respectively, t_{10} and t_{70} refer to the time when DO reaches 10% and 70% saturation (min), respectively.

The oxygen-transfer coefficient is adjusted to 20 °C as follows [62]:

$$K_L a_{20} = \frac{K_L a_{T_w}}{1.024^{T_w - 20}} \tag{2.5}$$

where $K_L a_{20}$ denotes the oxygen-transfer coefficient at 20 °C and T_W is water temperature (°C).

The oxygen-transfer coefficient is usually determined for tap water. Thus, for the water in which the experiment of the aerator is conducted, the correction factor is introduced. The α value is the ratio between the oxygen-transfer coefficients of the mechanical aerator in the tested and tap water, which is defined as [62]:

$$\alpha = \frac{K_L a_{20}\ test}{K_L a_{20}\ tap} \tag{2.6}$$

As the aerator is tested in pond water, the adjusted oxygen-transfer coefficient is computed as [62]:

$$K_L a'_{20} = \frac{K_L a_{20}}{\alpha} \tag{2.7}$$

The standard oxygen-transfer rate for an aerator is calculated via its oxygen-transfer coefficient as [62]:

$$SOTR = K_L a_{20} \cdot C_s^{20} \cdot V_{pond} \cdot 10^{-3} \tag{2.8}$$

where $SOTR$ stands for the standard oxygen-transfer rate (kg/h), C_s^{20} refers to the concentration of DO at saturation and 20 °C, V_{pond} is the pond volume (m^3), and 10^{-3} is converting factor from grams to kilograms.

The standard aeration efficiency of aerators is the ratio between the standard oxygen-transfer rate and the power applied, which is defined as:

$$SAE = \frac{SOTR}{P_{MA}} \tag{2.9}$$

where SAE is the standard aeration efficiency (kg/kWh) and P_{MA} represents the power applied to the aerator (kW).

2.4.4 Types of Aerators

Mechanical aerators used in aquaculture are modified from wastewater treatment aerators; hence, they are of the same design features as well as functions. Vertical pump sprayers and paddlewheel aerators, which belong to splashed aerators, splash water into the air. Bubble aerators, e.g., diffused-air systems and propeller-aspirator-pump aerators, release air bubbles into the water.

Figure 2.1 Diffused air aeration system [19].

Diffused-air aerators, which are illustrated in Fig. 2.1, have air blowers with low pressure and high volume to blow the air via fine-bubble diffusers positioned at the pond bottom or suspended in the water. There are many types of diffused-air systems such as air compressors, blowers, ceramic dome diffusers, and porous ceramic tubing; their application in shrimp aquaculture, however, is not so popular [63]. Otherwise, they are utilized in laboratories and hatcheries. The diffused-air systems accomplish high efficiency in transferring oxygen bubbles from the air to water as the water column in the pond is deep enough to provide sufficient contact time of air bubbles in water ponds. As a result, diffused-air aerators function more efficiently with deep ponds than shallow ponds [11].

Propeller-aspirator-pump aerators are floating-surface devices shown in Fig. 2.2, including such main components as an electric motor, a hollow, and a rotating shaft enclosed in a housing. An air diffuser is connected to the end of the housing. An impeller, which is attached to the end of the rotating shaft, rotates at high velocity to create a vacuum in the housing by pushing water through the end of the hollow shaft. As the pressure in air is higher than that in the housing, the air at the gas-liquid interface is drawn through a hollow shaft, and the air bubbles are injected into the water pond after released from the diffuser. The propeller-aspirator pump is considered a useful water-mixing device [63].

Figure 2.2 Propeller-aspirator pump [19].

Vertical pump sprayers, which are illustrated in Fig. 2.3, comprise of a submerged electrical motor and a propeller, which are suspended inside the float. The propeller, which is connected to a shaft beneath the water surface, rotates at 1730 or 3450 rpm to force water up to the air to make aeration [11]. The vertical pump sprayer could only enhance the oxygen content in its proximity, while water regions far away from the aerator are not oxygenated. Furthermore, only the water near the surface is splashed into the atmosphere. For this reason, this type of aerator is commonly employed in small and shallow shrimp ponds or combined with other types of aerators [63].

Figure 2.3 Vertical pump sprayer [19].

Among mechanical aerators, paddlewheel aerators shown in Fig. 2.4 are commonly used in shrimp farming [55], especially Taiwanese style aerators [16]. Their main components involve an electric motor and paddlewheels attached to a rotating shaft. The paddlewheels are suspended by floating units. The capacity of electric motors ranging from 0.8 to 2 kW is preferred for small ponds [63], with revolutions at 1750 rpm [11]. A gearbox, nevertheless, is utilized to decrease the speed of the motor shaft so that paddlewheels rotate at 70-120 rpm [11]. Rotating paddlewheels splashes the water into the air to cause aeration. In comparison with other types of aerators, paddlewheel aerators are of high efficiency in oxygen transfer [64].

Figure 2.4 Paddlewheel aerators [19].

Pure oxygen contact systems, which are rarely used for shrimp aquaculture, supply pure oxygen into the water pond. The culture systems aerated by pure oxygen could increase the carrying capacity and productivity [65]; nevertheless, oxygen transportation from suppliers to shrimp farms not only raises the extra cost but also increases the associated greenhouse gas emissions.

3. Sustainable Hybrid Energy Systems for Shrimp Farms

3.1 Potential of Renewable Energy Resources in the Mekong Delta

Most shrimp farms are located in the Mekong Delta, especially in coastal provinces in the western part of the delta. In remote areas in which the national power system is not present, or electric power supply is seriously insufficient; as a result, diesel engines have been employed to run mechanical aerators or to serve as backup power. Nevertheless, gasoline generators are of a levelized cost of 30,560 VND/kWh (1.3 USD/kWh), which is much more expensive than solar photovoltaic power 14,170 VND/kWh (0.6 USD/kWh) and wind power 10,100 VND/kWh (0.43 USD/kWh), respectively [66]. In addition, emissions from diel fuel cause environmental pollutions.

The Mekong Delta is of abundant renewable energy resources, particularly solar and wind energy. The solar energy intensity on average in a day could obtain 5 kWh/m^2 [67]. Besides, the wind intensity is strong thanks to the long coastal line towards both west and east sea, with the average wind speed fluctuating between 5.6 m/s to 6.0 m/s [68]. According to the national energy development vision until 2050 approved by the Vietnamese Prime Minister, the application of green energy resources will be investigated, and power supply is forecasted to constitute about 43% by renewable energy resources by 2050 [69]. In other words, hybrid solar and wind power systems seem beneficial and a promising solution to offer sustainable energy to replace conventional power resources for the shrimp industry in the Mekong Delta.

3.2 Proposed System Configuration

The sustainable hybrid energy system for aeration at shrimp farms is illustrated in Fig. 3.1, which depicts the proposed system in the constructional details. The constituents of the system are divided into power resources, power load, and shrimp ponds. The power resources consist of photovoltaic arrays and wind turbines, and national network as backup power in on-grid operation mode. Furthermore, the main power load of the system is the alkaline electrolyzer whilst the baseload involves illuminating load, water treatment system, and water pumps. The alkaline electrolyzer is chosen to produce oxygen onsite for aeration because alkaline electrolyzers have

been manufactured in the range of megawatts with a suitable price, making them the most popular application in terms of electrolysis technology at commercial levels [70].

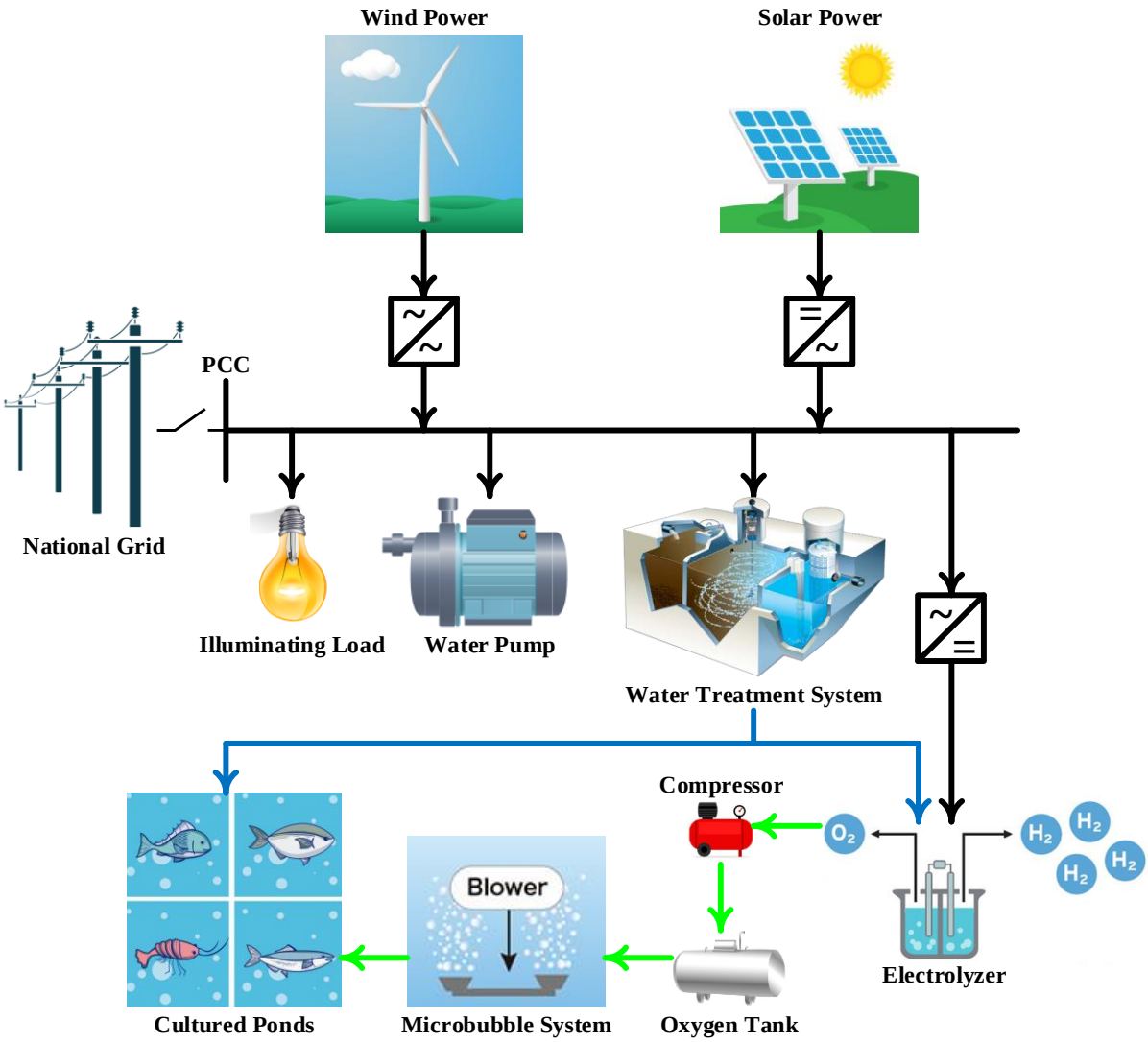

Figure 3.1 Sustainable hybrid energy system for aquaculture farms.

3.3 System Operation

Aeration for shrimp ponds runs continuously to sustain good water quality and gain biomass during the day, although it is required more at night than in the daytime. In the daytime, the primary power extracted from solar panels and wind turbines is converted to AC and imparted to the aeration system. The baseload is supplied by stable power since the water treatment system needs smooth power to produce clean water for electrolysis and cultured ponds. Apart from that, in order to provide clean water for the system, a low-cost water treatment technology, which is detailed in [71], is adopted. The remaining power is used to run the alkaline electrolyzer for producing oxygen in situ. Moreover, the by-product hydrogen through water electrolysis is utilized

for various applications, such as selling to the fertilizer factories or storing in the tank for generating backup power.

The pure oxygen from the electrolyzer is compressed via a short-term oxygen tank by a low-pressure compressor to the microbubble system at the bottom of ponds, which generates oxygen microbubbles for shrimps. The innovative aeration system, which is oxygenated by pure oxygen microbubbles with high oxygen absorption efficiency above 90% [72] instead of oxygen from the air, requires less energy demand and releases less emission compared to the conventional aeration system since the stripping of a great volume of nitrogen from the air is eluded, resulting in curtailing the amount of gas injected to shrimp ponds as well as reducing the energy requirement for compressors by a factor of five [73].

The fluctuation of DO in cultured ponds is caused by total respiration of sediment, plankton, and species under culture, photosynthesis production, and exchanges with the atmosphere. The DO requirement during daytime in shrimp ponds is low due to oxygen supplement from photosynthesis, corresponding with low power demand from the electrolyzer. Consequently, the electrolyzer is controlled to change its input power between 20% and 100% of its capacity according to the amount of DO in culture ponds [74]. When the sustainable hybrid energy system is well controlled, the energy demand is reduced, leading to low operation cost; in addition, the surplus electricity is sold to the national grid via point of common coupling (PCC) based on feed-in-tariffs (FITs) policy in Vietnam [75].

Aeration becomes essential at night since the DO level drops significantly during the night due to the cease activity of photosynthesis and respiration of organisms in the pond. The DO variations in shrimp ponds should be kept around 5 mg/L to provide suitable conditions for healthy growth [17]. For this reason, it is necessary to keep sufficient DO concentration to protect shrimp from low-oxygen mortality. Doubtlessly, in such condition only wind turbine system might not produce enough energy for the power demand of the system, especially the electrolyzer due to the high amount of oxygen demand or at daylight hours when renewable resources cannot satisfy the power load demand due to the volatility of these resources, the deficiency in power is inevitable. In other words, when the imbalance occurs, the energy storage system is employed to compensate for the mismatch of the system in islanded operation mode.

The configuration of components in the energy storage system, as well as its operation, depends on the applications of the by-product hydrogen.

3.3.1 Hydrogen Used for Commercial Purposes

When the by-product hydrogen is sold to the local fertilizer factories, which produce ammonia as fertilizer for agriculture, the energy storage system includes a battery bank and a diesel generator as a backup power supply.

The sustainable hybrid system in this context is depicted in Fig. 3.2. When the power deficiency occurs, the battery is discharged to satisfy the power shortage of the system. Nonetheless, if the load demand is beyond the capacity of the battery bank, the diesel generator is started to compensate for the energy mismatch of the system. When the system is connected to the national network, the shortage power is purchased via the power grid regardless of both battery and diesel generator.

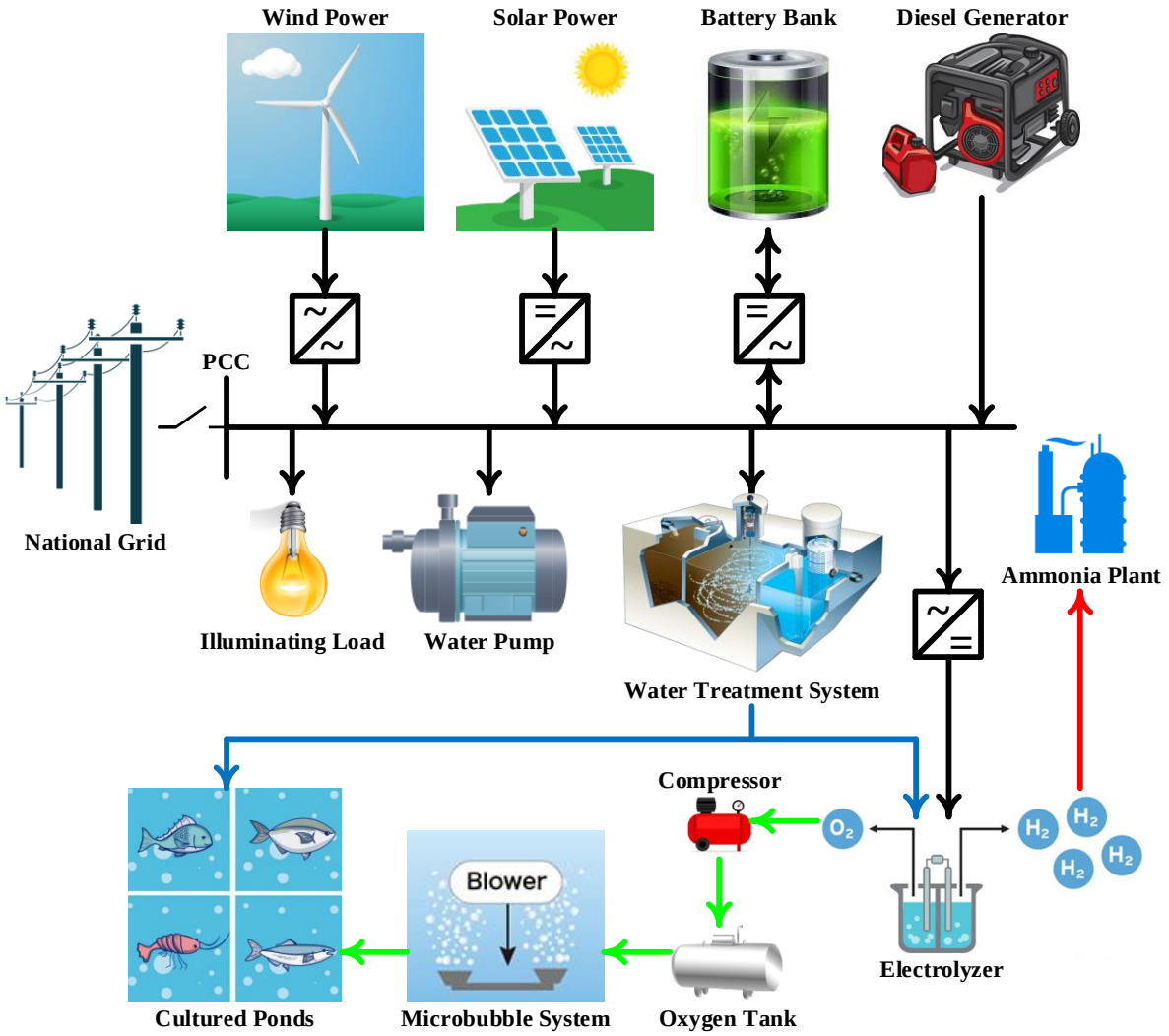

Figure 3.2 Sustainable hybrid energy system for aquaculture farms when hydrogen is sold to the fertilizer plant.

3.3.2 Hydrogen Used for Backup Power

When the by-product hydrogen from the electrolyzer is used to generate additional power for the system, the sustainable hybrid energy system having the proton-exchange membrane fuel cell (PEM-FC) and hydrogen storage tank as an energy storage system is presented in Fig. 3.3. When the power shortage occurs, the by-product hydrogen through the electrolysis process, which is compressed and stored in a hydrogen tank, is fed into PEM-FC to regenerate electric power to supply electrolyzer and baseload, compensating the energy mismatch of the system in islanded operation mode. Nevertheless, if the power demand is higher than the capacity of the fuel cell, the system is connected to the national network to purchase electricity, ensuring the stable operation of the system.

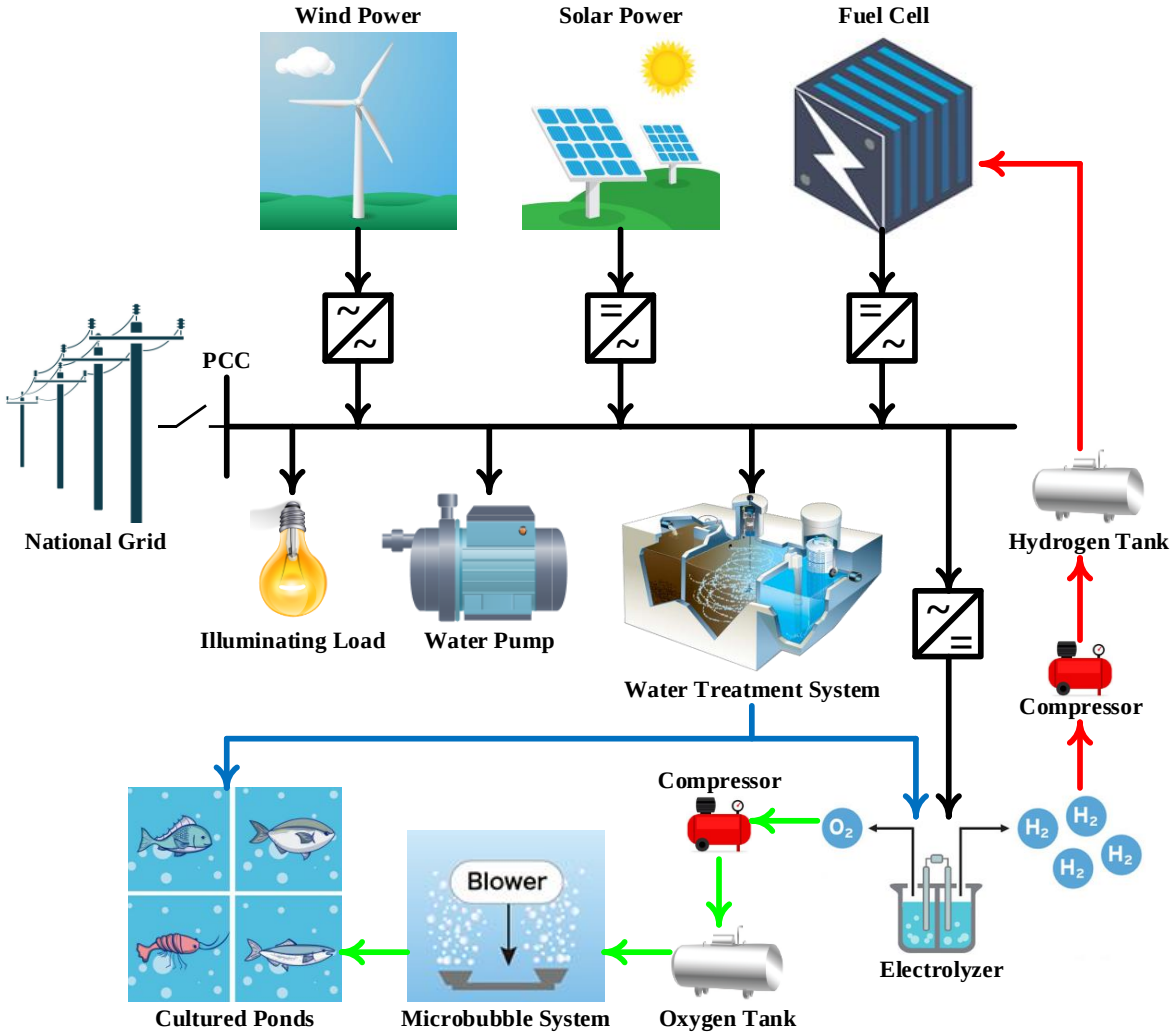

Figure 3.3 Sustainable hybrid energy system for aquaculture farms when hydrogen is used for backup power.

3.4 Power Management Strategy

The proposed strategy of power management for the system is necessary for managing the power distribution amongst energy resources, energy storage devices, and the power load to adapt to volatile behaviors of renewable resources and load demand. The strategy is designed to meet the power load demand by power produced from renewable resources as well as energy storage systems whilst the national power grid is considered as a backup power supply in on-grid mode. The system's power flow is strictly controlled by comparing the generated power to the load demand, as shown in Fig. 3.4 and Fig. 3.5.

The imbalance between power generated from renewable resources P_{gen} (W) and power load demand P_{load} (W) at an instant time is expressed by:

$$P_{im}(t) = P_{gen}(t) - \frac{P_{load}(t)}{\eta_{inv}} \tag{3.1}$$

where P_{im} is the imbalance power (W) and η_{inv} presents the inverter efficiency.

The working strategy of the hybrid system is determined by the imbalance of renewable power and its system configurations.

3.4.1 Hydrogen Used for Commercial Purposes

The control strategy in this context, which is shown in Fig. 3.4, prioritizes the energy produced from solar PV panels and wind power system or stored in the battery bank to satisfy the load demand and consider diesel generator as a backup in autonomous operation mode whilst the power deficiency is met by the national grid in grid-connected mode.

If the generated power from renewable energy is adequate and higher than load demand, the load is served directly by the PV system and wind turbine system; moreover, the surplus power is used to charge the battery bank in islanded mode or sold to the national grid in grid-connected mode. In islanded mode, if there is excessive power after the battery is fully charged, the remaining power is dumped. The sold and dump power is calculated as:

$$\begin{cases} P_{gs}(t) = P_{im}(t) \\ P_{d}(t) = P_{im}(t) - P_{ch}(t) \end{cases} \tag{3.2}$$

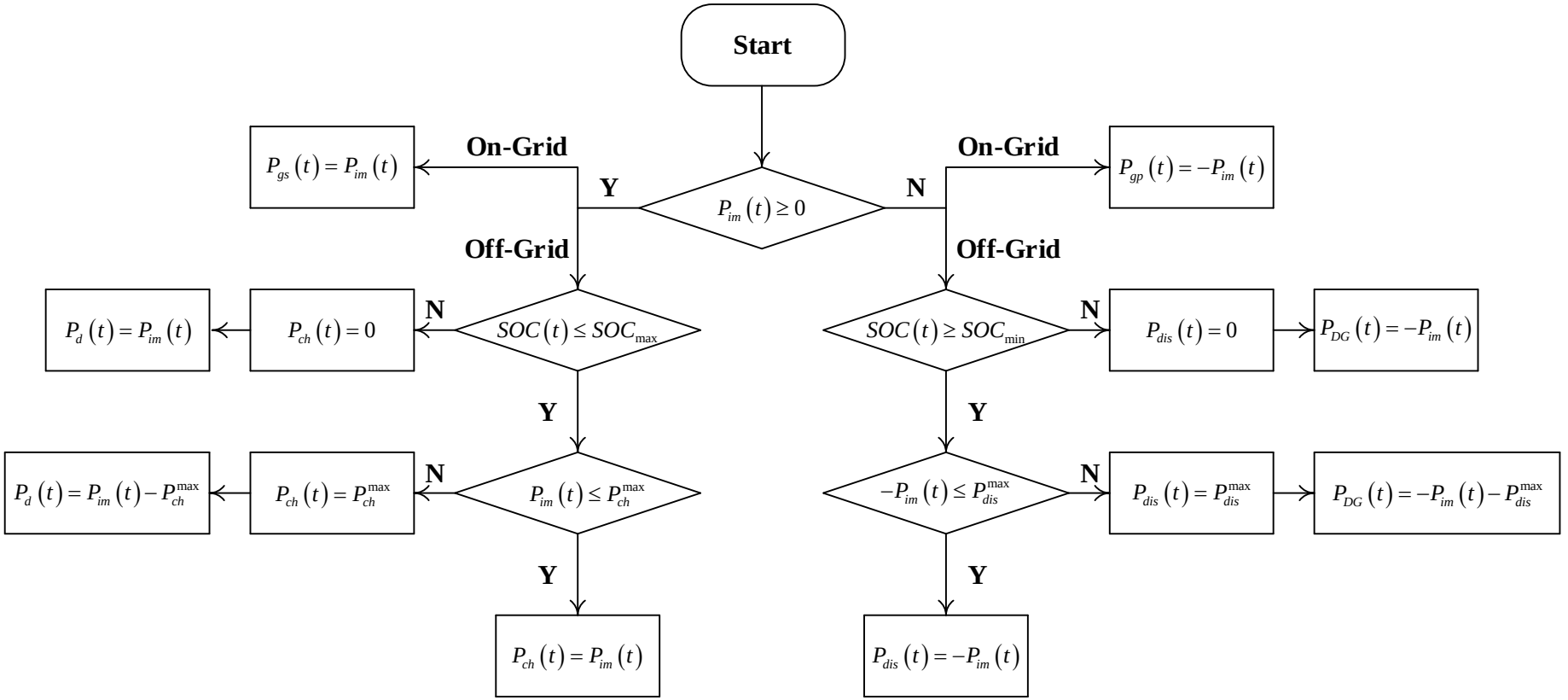

Figure 3.4 Flowchart of power management strategy when hydrogen is used for commercial purposes.

where P_{ch} is the charging power (W), P_{gs} and P_d are the power sold to the national grid and dumped (W), respectively.

In islanded mode, if the generated power is not sufficient to cover the power demand, the battery bank is discharged to supply enough power to the system. However, if the power load is higher than the maximal capacity of the battery bank after its full discharge, the power deficiency is presumed to be entirely supplied by a diesel generator. Besides, in grid-connected mode, the power shortage might be purchased from the national power system, which is assumed to be of reliability of 100% and can be expressed as follows:

$$\begin{cases} P_{DG}(t) = -P_{im}(t) - P_{dis}(t) \\ P_{gp}(t) = -P_{im}(t) \end{cases} \quad (3.3)$$

where P_{dis} is discharging power (W), P_{DG} and P_{gp} are real output power of diesel generator (kW) and power purchased from the grid (W), respectively.

3.4.2 Hydrogen Used for Backup Power

When the self-product hydrogen is stored in the tank for generating additional power, the working strategy of the hybrid system is illustrated in Fig. 3.5.

If the generated power by wind turbines and PV arrays is higher than load demand, the excess of renewable energy is sold to the national network in on-grid mode or dumped in autonomous mode. The sold power and the dumped power are computed as follows:

$$\begin{cases} P_{gs}(t) = P_{im}(t) \\ P_{d}(t) = P_{im}(t) \end{cases} \quad (3.4)$$

Besides, the fuel cell stops due to the surplus of electricity. The control system checks the hydrogen level in the tank. If the hydrogen tank level is lower than the maximum level of hydrogen $C_{H_2}^{\max}$ (kg) in the storage tank, the hydrogen flow produced from electrolyzer is fed directly to the tank until the tank reaches its capacity and the surplus hydrogen $m_{H_2}^{dumped}$ (kg) is dumped to the temporary tank, being sold for different applications. A compressor is widely used to fill hydrogen to the tank; however, the electrolyzer might be designed to provide high pressure [76]. Notably, the PEM electrolyzer could operate with the pressure up to 200 bar [77].

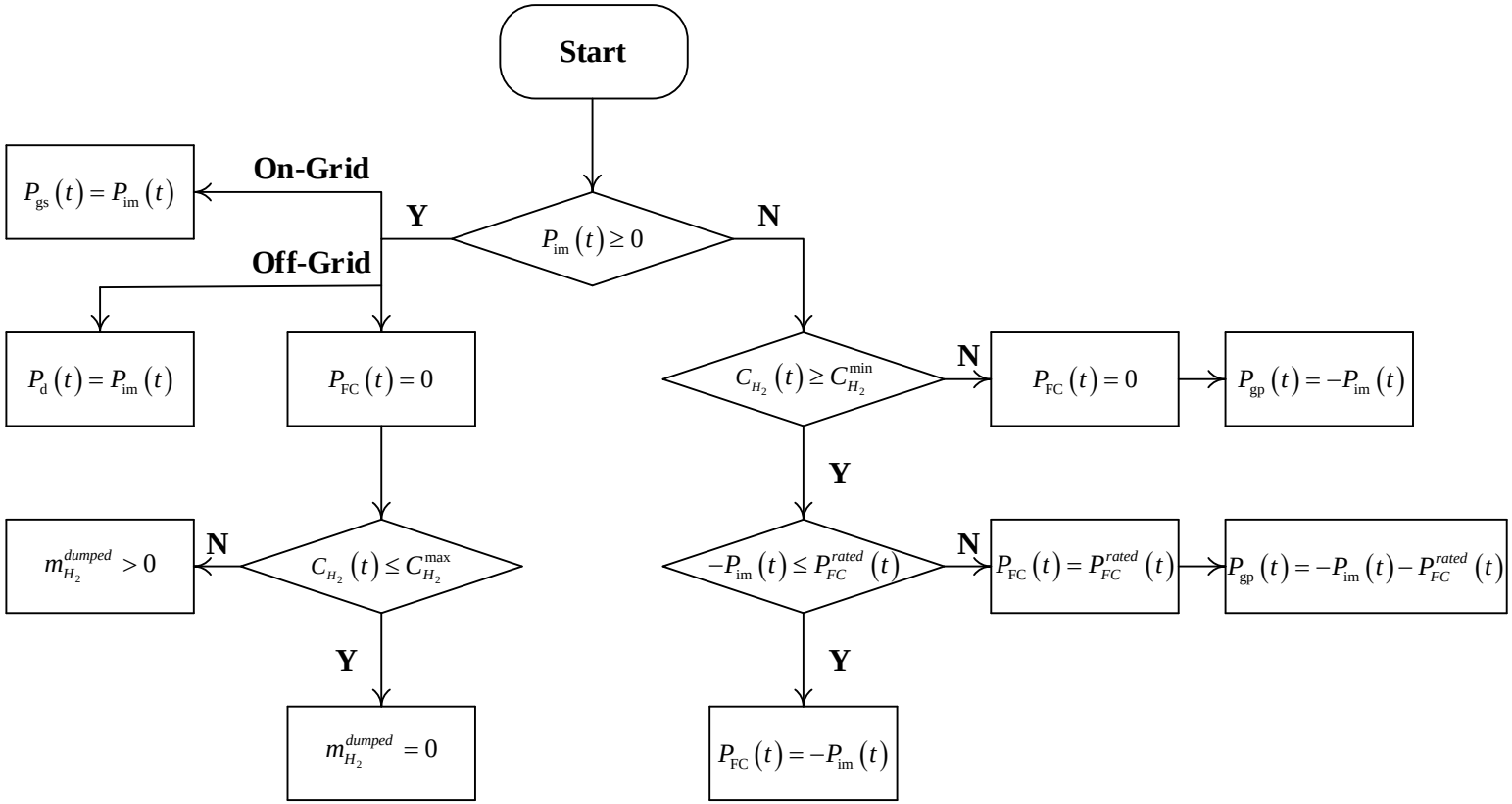

Figure 3.5 Flowchart of power management strategy when hydrogen is used for backup power.

When renewable energy might not meet the load demand, the fuel cell is harnessed. Nevertheless, the amount of unmet power is purchased directly from the national grid, with reliability being assumed 100% when the fuel cell might not work due to a lower level of hydrogen compared to the minimum level of hydrogen $C_{H_2}^{\min}$ (kg) in the storage tank. On the contrary, the fuel cell produces enough power to meet the demand. Nonetheless, if the power demand is higher than the capacity of the fuel cell P_{FC}^{rated} (W), the power shortage is provided by the national network to prevent the loss of power supply. The purchasing power from the national grid might be obtained by:

$$P_{gp}(t) = -P_{im}(t) - P_{FC}(t) \tag{3.5}$$

where P_{FC} presents the output power of fuel cell (W).

4. Optimal Design on Sustainable Hybrid Energy Systems by Multiobjective Functions

4.1 Power Load Model (PL)

4.1.1 Dissolved Oxygen Model (DO)

The changing rate of DO level in a cultured pond affected by photosynthesis production, total respiration of organisms, and exchange with the atmosphere is expressed as:

$$\frac{dDO}{dt} = P_{O_2}(t) - R_{O_2}(t) \pm E_{O_2}(t) \tag{4.1}$$

where dDO/dt is the changing rate of DO level ($mgL^{-1}h^{-1}$), P_{O_2} denotes photosynthesis production ($mgL^{-1}h^{-1}$), R_{O_2} presents total respiration of organisms ($mgL^{-1}h^{-1}$), and E_{O_2} refers to the oxygen exchange rate ($mgL^{-1}h^{-1}$).

The oxygen exchange rate between the air and the water surface depends on the wind speed over the pond and the concentration difference from saturation. The re-aeration rate is defined as [78]:

$$E_{O_2} = \frac{\alpha_j}{z_1} \cdot K_L \cdot (C_s - C_t) \tag{4.2}$$

where α_j is the dimensionless re-aeration adjustment coefficient, z_1 denotes the control volume thickness affected by re-aeration (m), C_s indicates DO concentration at saturation, C_t refers to the instantaneous DO concentration (mg/L), and K_L is the oxygen transfer coefficient from wind (m/h), which is determined by the following equation [79]:

$$K_L = 0.0036 \cdot \left(8.43 \cdot \sqrt{v} - 3.67 \cdot v + 0.43 \cdot v^2\right) \tag{4.3}$$

where v is the wind speed above the water interface of the pond (m/s).

Nevertheless, the re-aeration is disregarded due to the negligible wind speed on the pond surface.

The amount of oxygen produced by photosynthesis depends on such ambient factors as the intensity of photosynthetically active solar radiation (PAR) and water temperature together with the concentration of chlorophyll-a, which is given as [80]:

$$P_{O_2}(t) = 9.6 \cdot \alpha_{par} \cdot R_S(t) \cdot 1.036^{(T_w(t)-20)} \cdot e^{(1-\alpha_{par} \cdot R_S(t))} \cdot Chla \quad (4.4)$$

where α_{par} indicates the ratio of PAR to broadband solar radiation of investigated sites (m^2/kW), R_S refers to the broadband solar radiation (kW/m^2), T_W denotes water temperature of the pond (°C), and $Chla$ presents the concentration of chlorophyll-a in the pond (mg/L).

The total respiration rate in a pond involving the respiration rate of aquatic species under culture, namely fish or shrimp, sediment respiration due to decaying organic matter, and water respiration caused by phytoplankton is provided by the following equation:

$$R_{O_2}(t) = R_{species}(t) + R_{sediment}(t) + R_{water}(t) \quad (4.5)$$

where $R_{species}$ is the respiration rate of species under culture ($mgL^{-1}h^{-1}$), $R_{sediment}$ is the sediment respiration rate ($mgL^{-1}h^{-1}$), R_{water} is the water respiration rate ($mgL^{-1}h^{-1}$).

Under semi-intensive to intensive culture conditions, the average value of water respiration rate in brackish water ranges between 0.01 and 0.86 ($mgL^{-1}h^{-1}$) while the sediment respiration rate is of values from 0.3 to 0.56 ($mgL^{-1}h^{-1}$) [81].

Regarding the cultured species respiration rate, the total respiration rate of shrimp is expressed as follows:

$$R_{shrimp}(t) = f\left(T_w, S, m_{shrimp}, St_{shrimp}\right) \quad (4.6)$$

where the individual shrimp's oxygen consumption rate, which is tabulated in [82], is a function of water temperature T_w (°C), salinity in the pond S (ppt), and wet body weight m_{shrimp} (g). The oxygen consumption rate of shrimp per one cubic meter of water is calculated by multiplying the individual respiration rate and the stocking density of shrimp in that volume St_{shrimp} [60].

The total demand of oxygen for a pond is given by:

$$TOD(t) = \left(R_{O_2}(t) - P_{O_2}(t)\right) \cdot V_{pond} \cdot 10^{-3} \quad (4.7)$$

where TOD is total oxygen demand for the pond (kg/h).

The total oxygen demand in the shrimp pond is used to characterize the power requirement of the alkaline electrolyzer. The total oxygen respiration, which is assumed constant during the day, is utilized to determine the power capacity of alkaline electrolyzer whilst the DO fluctuation in the pond due to the photosynthesis process affects the operation of the electrolyzer.

4.1.2 Power Capacity of Electrolyzer

The power capacity of electrolyzer is computed according to the total oxygen demand of the pond, which is converted to the oxygen production flow rate from the electrolyzer by the following equation [83]:

$$Q_{O_2}(t) = 0.6999 \cdot \frac{TOD(t)}{\eta_\mu} \tag{4.8}$$

where Q_{O_2} is the total oxygen flow rate (Nm^3/h) and η_μ is the oxygen absorption efficiency generated by the microbubble system.

The required power to operate the electrolyzer is expressed as follows [84]:

$$P_{ELZ} = U_c \cdot N_c \cdot I_{ELZ} = U \cdot I_{ELZ} \tag{4.9}$$

where P_{ELZ} is the power required by electrolyzer (W), U_c represents the cell's actual voltage (V), N_c is the number of cells in an electrolyzer's stack, I_{ELZ} is the operating current of electrolyzer (A), and U is the supplied voltage (V).

On the one hand, the total hydrogen flow rate produced from electrolyzer is given by [85], [86]:

$$Q_{H_2} = 80.69 \cdot \eta_F \cdot \frac{N_c \cdot I_{ELZ}}{n_{H_2} \cdot F} = 80.69 \cdot \eta_F \cdot \frac{N_c \cdot P_{ELZ}}{U \cdot n_{H_2} \cdot F} \tag{4.10}$$

where Q_{H_2} is the hydrogen gas flow rate (Nm^3/h), η_F refers to Faradic efficiency, n_{H_2} indicates the number of electrons transferred hydrogen molecule ($n_{H_2} = 2$), and F is the Faraday's number (96485 C/mol).

On the other hand, the oxygen and hydrogen flow rates produced from the electrolysis process are provided by the following equations [86]:

$$Q_{H_2} = \frac{J \cdot A}{2 \cdot F} \tag{4.11}$$

$$Q_{O_2} = \frac{J \cdot A}{4 \cdot F} \tag{4.12}$$

where J is the current density (A/cm^2) and A is the membrane-electrode-assembly area (cm^2).

It can be seen from (4.9) and (4.10) that the hydrogen flow rate from the electrolysis process is double the oxygen rate. As a result, the power capacity of electrolyzer can be determined from (4.6), (4.7), (4.8), (4.9), and (4.10) as follows:

$$P_{ELZ} = \frac{2 \cdot n_{H_2} \cdot F \cdot U_c \cdot Q_{O_2}}{80.69 \cdot \eta_F} \tag{4.13}$$

The DO level in cultured ponds rises during the day because the amount of oxygen produced from the photosynthesis process is higher than that of the respiration rate. On the contrary, when the photosynthesis process ceases at night, DO decreases due to the respiration of organisms in the pond. According to the changes in DO concentration in the pond, the electric power required to run the electrolyzer to maintain a stable DO level is also computed by (4.11).

4.1.3 Power Capacity of Mechanical Aerator

In order to compare the features of the innovative aeration system with the conventional aeration system run by mechanical aerators, the electrical power requirement for mechanical aerators is taken into account.

Under various operation conditions of the pond, the actual aeration efficiency of aerators might be expressed by following equation [87]:

$$AAE = \frac{\alpha \cdot SAE \cdot \left(\beta \cdot C_s - C_p\right) \cdot 1.024^{(T_w - 20)}}{9.07} \tag{4.14}$$

where AAE refers to the actual aeration efficiency of aerator (kg/kWh), β presents the ratio of DO saturation concentration of pond water to DO saturation concentration of tap water, and C_p is the initial concentration in pond water at temperature T_w (°C).

The power required by mechanical aerator is computed according to the total oxygen demand and its aeration efficiency by the following expression [88]:

$$P_{MA} = \frac{TOD}{AAE} \tag{4.15}$$

4.2 Solar Photovoltaic Model (PV)

The output power generated hourly from the PV system is dependent on ambient factors (solar radiation, air temperature, and wind speed) as well as the module's performance. The mathematical presentation employed to compute the output power of the system is provided by [89]:

$$\begin{aligned} P_{PV}(t) = \eta_{PV}^{STC} \cdot \Bigg[& 1 + \frac{\mu_{PV}}{\eta_{PV}^{STC}} \left(T_a(t) - T_{STC} \right) \\ & + \frac{9.5 \cdot \mu_{PV} \cdot \left(T_{NOC} - 20 \right) \cdot \left(1 - \eta_{PV}^{STC} \right)}{800 \cdot \eta_{PV}^{STC} \cdot \left(5.7 + 3.8 \cdot v(t) \right)} \cdot G(t) \Bigg] \cdot A_{PV} \cdot G(t) \end{aligned} \tag{4.16}$$

where P_{PV} is the output power of PV system (W), η_{PV}^{STC} presents the module efficiency at standard test condition (STC) (%), μ_{PV} indicates the temperature coefficient of the output power (%/°C), T_{STC} refers to the STC temperature (25 °C), T_{NOC} denotes the nominal operating cell temperature (°C), A_{PV} denotes the area of the PV module (m^2), and G refers to the global solar radiation on the tilted surface (W/m^2), which is computed with the following equation [90]:

$$G(t) = G_b(t) + G_d(t) + G_r(t) \tag{4.17}$$

where G_b, G_d, and G_r are the beam, diffuse, and reflected components of the global solar radiation (W/m^2), respectively.

The beam radiation on the tilted surface is calculated by [90]:

$$G_b(t) = \frac{G_g^h(t) - G_d^h(t)}{\cos\left(90 - \alpha_s\right)} \cdot \cos\theta \tag{4.18}$$

where G_g^h and G_d^h are the global horizontal radiation and the diffuse horizontal radiation (W/m^2), respectively, α_s is the solar altitude (°), and θ is the angle of incidence (°).

The diffuse radiation on the tilted surface is computed by [90]:

$$G_d(t) = G_d^h(t) \cdot \frac{1 + \cos\beta_t}{2} \tag{4.19}$$

where β_t is the tilt angle (°).

The reflected radiation on the tilted surface is given by [90]:

$$G_r(t) = \rho_g \cdot G_g^h(t) \cdot \frac{1-\cos\beta_t}{2} \tag{4.20}$$

where ρ_g is the ground reflectance.

4.3 Wind Turbine Model (WT)

The hourly generated power by a wind turbine system is expressed as a function of available wind velocity at a specific hub height of the wind turbine by the following equation [91]:

$$P_{WT}(t) = \begin{cases} 0 & (v < v_i \text{ or } v > v_o) \\ \eta_{WT} \cdot P_{WT}^{rated} \cdot \dfrac{v^3(t) - v_i^3}{v_r^3 - v_i^3} & (v_i \le v \le v_r) \\ \eta_{WT} \cdot P_{WT}^{rated} & (v_r \le v \le v_o) \end{cases} \tag{4.21}$$

where P_{WT} denotes the power produced by WT system (W), P_{WT}^{rated} is the rated power of WT (W), v_r, v_i, and v_o are the rated, cut-in, and cut-out wind speed (m/s), respectively, η_{WT} is the efficiency of the WT system, which is presented as [92]:

$$\eta_{WT} = \eta_g \cdot \eta_b \tag{4.22}$$

where η_g is the generator efficiency and η_b is the gearbox/bearing efficiency.

The actual wind turbine power output at a specific site directly correlates to the wind speed at particular hub height and wind characteristics of the turbine. Hence, the wind speed measured at a reference hub height should be converted to the desired hub height by using logarithmic law as follows [93]:

$$v = v_{ref} \cdot \frac{\ln(h / z_0)}{\ln(h_{ref} / z_0)} \tag{4.23}$$

where v is the wind speed at hub height (m/s), v_{ref} is the measured wind speed at reference height (m/s), h is the hub height (m), h_{ref} is the reference height (m/s), and z_0 stands for the surface roughness length (m).

4.4 Battery Bank Model (BB)

When the generated power is higher than the load demand, the battery is in the charging state with the following formulation [94]:

$$SOC(t) = SOC(t-1)\cdot(1-\sigma_{BB}) + P_{im}(t)\cdot\eta_{BB}/E_{BB} \tag{4.24}$$

where $SOC(t)$ and $SOC(t-1)$ are the states of charge of battery bank at the time t and $t-1$, respectively, σ_{BB} is hourly self-discharge rate, E_{BB} is the battery bank capacity (Wh), and η_{BB} denotes the efficiency of the battery bank.

In contrast, when the generated power is smaller than the load demand, the battery is in discharging state with the following formulation [94]:

$$SOC(t) = SOC(t-1)\cdot(1-\sigma_{BB}) + P_{im}(t)/(\eta_{BB}\cdot E_{BB}) \tag{4.25}$$

4.5 Fuel Cell Model (FC)

The amount of hydrogen consumed by a fuel cell depends on its output power, as shown in the following expression [95]:

$$m_{H_2}^{cons}(t) = \begin{cases} \alpha_{FC}\cdot P_{FC}^{rated} + \beta_{FC}\cdot P_{FC}(t) \\ \left(P_{FC} \le P_{eff}^{\max}\cdot P_{FC}^{rated}\right) \\ \alpha_{FC}\cdot P_{FC}^{rated} + \beta_{FC}\cdot P_{FC}(t)\cdot\left[1+F_{eff}\cdot\left(\dfrac{P_{FC}(t)}{P_{FC}^{rated}} - P_{eff}^{\max}\right)\right] \\ \left(P_{eff}^{\max}\cdot P_{FC}^{rated} < P_{FC} < P_{FC}^{rated}\right) \end{cases} \tag{4.26}$$

where $m_{H_2}^{cons}$ is the hourly fuel consumption of FC (kg/h), α_{FC} and β_{FC} are the coefficients of hydrogen consumption curve (kg/kWh), P_{FC}^{rated} and P_{FC} are the capacity and output power of FC (W), respectively, $P_{eff}^{\max}$ is the power of maximum efficiency, and F_{eff} is the correction factor considering the high consumption above $P_{eff}^{\max}$. The FC efficiency ranges between 31% and 46% [95].

4.6 Hydrogen Tank Model (HT)

The hydrogen gas flow produced from the electrolyzer might be stored in the forms of compressed high-pressure gas, liquid, or hydrogen-absorbing materials.

The level of hydrogen in the storage tank is written as follows [96]:

$$C_{H_2}(t) = C_{H_2}(t-1) + m_{H_2}^{prod}(t) - m_{H_2}^{cons}(t)/\eta_{HT} \quad (4.27)$$

where $C_{H_2}(t)$ and $C_{H_2}(t-1)$ refer to the states of the hydrogen mass in the storage tank (kg/h) at the time t and $t-1$, respectively, $m_{H_2}^{prod}$ is the hydrogen mass flow produced from electrolyzer hourly (kg/h), and η_{tank} is the storage efficiency.

4.7 Diesel Generator Model (DG)

The diesel generator is required to provide backup power for the autonomous system in the case of power deficiency. Moreover, the fuel consumption rate of diesel generator, which directly decides the amount of greenhouse gas emissions and operation cost, is written as follows [97]:

$$FC_{DG}(t) = c_1 \cdot P_{DG}^{rated} + c_2 \cdot P_{DG}(t) \quad (4.28)$$

where FC_{DG} is the fuel consumption rate of diesel generator (L/h), P_{DG}^{rated} and P_{DG} are the rated and real output power of diesel generator (kW), respectively, c_1 and c_2 denote the intercept coefficient and slope of fuel consumption curve (L/kWh).

4.8 Objective Functions

4.8.1 Annualized Cost of System (ACS)

The annualized cost of the system, which is composed of the annualized cost of components in the system, the total cost of purchasing and selling electricity, and the total cost of selling surplus hydrogen, is computed by the following equation:

$$ACS = C_{ACC} + C_{GP} - C_{GS} - C_{HS} \quad (4.29)$$

where C_{ACC} is the annualized cost of components in the system, C_{GP} and C_{GS} are the total cost of purchasing and selling electricity, and C_{HS} is the total cost of selling surplus hydrogen.

The annualized cost of components in the system is calculated as follows:

$$C_{ACC} = C_{NPC} \cdot CRF(i, N) \quad (4.30)$$

where C_{NPC} is the net present cost or life-cycle cost and $CRF(i, N)$ denotes the capital recovery factor, used to convert the present value into a series of equal annual cash flows, having the mathematical formulation expressed as:

$$CRF\left(i,N\right)=\frac{i}{1-\left(1+i\right)^{-N}} \tag{4.31}$$

where N is the project lifetime (years) and i refers to the interest rate (%).

The net present cost involving the capital cost, the total maintenance cost, the total replacement cost, the total depreciation tax benefit, and the total salvage value incurred over the project lifetime.

$$C_{NPC}=C_{CAP}+C_{MAI}+C_{REP}-C_{DTB}-C_{SV} \tag{4.32}$$

where C_{CAP} indicates the capital cost, C_{MAI} presents the total maintenance cost, C_{REP} is the total replacement cost, C_{DTB} refers to the total depreciation tax benefit, and C_{SV} is the total salvage value.

The capital cost includes purchasing and installing the component.

The total maintenance cost is expressed as [98]:

$$C_{MAI}=\sum_{n=1}^{N}\frac{MAI}{\left(1+i\right)^{n}}\cdot\left(1-tr\right) \tag{4.33}$$

where n is the n-th year of the project, MAI refers to the annual maintenance cost, tr denotes the tax rate (%).

The total replacement cost is the cost of replacing any components of the system occurring during the lifetime and is computed as [98]:

$$C_{REP}=\sum_{r=1}^{R}\frac{REP}{\left(1+i\right)^{r\cdot l_c}}\cdot\left(1-tr\right) \tag{4.34}$$

where r refers to the r-th replacement with the total number of replacements R during the project lifetime, REP is the investment cost of the replaced component, and l_c denotes the lifetime of the replaced component (years).

The total depreciation tax benefit is defined as the present value of the depreciation tax benefit over the financed life of the project asset and is expressed as follows [98]:

$$C_{DTB}=\sum_{n=1}^{N}\frac{DTB}{\left(1+i\right)^{n}}\cdot tr \tag{4.35}$$

where DTB is the annual depreciation tax benefit, which is assumed to be straight-line based on [99].

The total salvage value, which is the value remaining of a component at the end of the project, is given by the following equation:

$$C_{SV} = \frac{SV}{(1+i)^N} \tag{4.36}$$

where SV is the salvage value, accounting for 10% of the initial cost [99].

The cost of power exchange between the advanced aeration system and the national network including the cost of purchasing electricity from the grid and the cost of selling surplus electricity to the grid during a year is defined as follows:

$$C_{GP} = \sum_{t=1}^{T} P_{gp}(t) \cdot c_{gp} \tag{4.37}$$

$$C_{GS} = \sum_{t=1}^{T} P_{gs}(t) \cdot c_{gs} \tag{4.38}$$

where T denotes the number of hours in a year (8760 hours), c_{gp} and c_{gs} are the purchasing and selling electricity price ($/kWh), respectively. In stand-alone operation mode, the cost of power exchange is neglected.

The by-product hydrogen is utilized for power generation; nevertheless, the surplus hydrogen, which is dumped due to the limited capacity of the hydrogen tank, is sold to fertilizer factories. The total cost of selling dumped hydrogen is given by:

$$C_{HS} = \sum_{t=1}^{T} m_{H_2}^{dumped}(t) \cdot c_{hs} \tag{4.39}$$

where c_{hs} is the selling price of hydrogen ($/kg).

The first objective function, which is an economic evaluation, is to minimize the ACS.

4.8.2 Loss of Power Supply Percentage (LPSP)

The second objective function, which is defined as the ratio between the total unmet load and the total power load demand, is applied to minimize the loss of power supply percentage according to equation [100]:

$$LPSP = \frac{\sum_{t=1}^{T} P_{unmet}(t)}{\sum_{t=1}^{T} P_{load}(t)} \tag{4.40}$$

where *LPSP* is the loss of power supply percentage used to evaluate the reliability of the system in islanded operation mode due to the stochastic nature of renewable energy resources and P_{unmet} is the unmet load at each hour (W), which is given by:

$$P_{unmet}(t) = \begin{cases} 0 & \left(P_{load}(t) < P_{total}(t)\right) \\ P_{load}(t) - P_{total}(t) & \left(P_{load}(t) > P_{total}(t)\right) \end{cases} \tag{4.41}$$

where P_{total} is the generated power from available resources (W).

4.8.3 Carbon Dioxide Emission (EMI)

The total amount of CO_2 emission from the national grid in case of grid-connected operation mode or diesel generator in the autonomous mode is minimized by the third objective function and expressed as:

$$EMI = \sum_{t=1}^{T} \left[P_{DG}(t) \cdot e_{DF} + P_{gp}(t) \cdot e_{grid} \right] \tag{4.42}$$

where EMI is the amount of CO_2 emission of the system during a year (t-CO_2), e_{grid} and e_{DF} are the grid and diesel fuel emission factors (g-CO_2/kWh), respectively.

When the system is connected to the national network, the emission from diesel generator is zero and vice versa in the islanded grid.

4.9 Multiobjective Optimization for Sustainable Hybrid Energy Systems

4.9.1 Constraints

The optimization problem attempts to achieve the optimal values of decision variable including tilt angle β_t (°), azimuth angle γ_a (°), PV peak capacity P_{PV}^{peak} (W_p), WT rated capacity P_{WT}^{rated} (W_r), battery bank capacity E_{BB} (Wh), FC rated capacity P_{FC}^{rated} (W_r), and the mass of HT m_{tank} (kg). The constraints should be met:

$$
\begin{aligned}
&0 \le \beta_t \le 90^\circ \\
&-180^\circ \le \gamma_a \le 180^\circ \\
&0 \le P_{PV}^{peak} \le P_{PV}^{\max} \\
&0 \le P_{WT}^{rated} \le P_{WT}^{\max} \\
&0 \le E_{BB} \le E_{BB}^{\max} \\
&0 \le P_{FC}^{rated} \le P_{FC}^{\max} \\
&0 \le m_{HT} \le m_{HT}^{\max}
\end{aligned}
\tag{4.43}
$$

where $P_{PV}^{\max}$, $P_{WT}^{\max}$, $E_{BB}^{\max}$, $P_{FC}^{\max}$, and $m_{HT}^{\max}$ denote the maximum values of PV capacity, WT capacity, BB capacity, FC capacity, and the mass of HT, respectively.

The PV system is of the maximum values of PV capacity according to the capacity potential, which depends on the packing factor, the available land of the investigated site, and the power over the module's unit area and is computed as [101]:

$$
P_{CP} = \frac{\sum_{j=1}^{m_j}\left(\sum_{i=1}^{n_i} S_{ij} \cdot SF_i\right) \cdot PF_j \cdot P_{PV}^{unit}}{1000} \tag{4.44}
$$

where P_{CP} is the capacity potential (kW), m_j presents the total number of pixels in the investigated area, n_i refers to the site use suitability category number ($n_i = 7$), S_{ij} denotes the area of site use type i in pixel j (m^2), SF_i indicates the suitable fraction of site utilization type i, P_{PV}^{unit} is the power per unit area of the PV array, and PF_j represents the packing factor, and expressed as [101]:

$$
PF = \frac{1}{\cos\beta_t + \frac{\sin\beta_t}{\tan\alpha_s} \cdot \cos\gamma_a} \tag{4.45}
$$

The packing factor fluctuating between 0 and 1 represents the effective area of PV panel per square meter of the site area.

Similarly, the maximum WT capacity is set the same as the maximum value of PV capacity.

Furthermore, in order to protect the battery bank from damage due to overcharging and discharging, the charging control limit and control strategy should be considered elaborately due to the high replacement cost of batteries [102], [103]. Hence, the physical constraints should follow the lower as well as the upper limit as:

$$\begin{cases} SOC_{\min} \le SOC(t) \le SOC_{\max} \\ P_{ch}(t) \le P_{ch}^{\max} \\ P_{dis}(t) \le P_{dis}^{\max} \end{cases} \quad (4.46)$$

where $SOC_{\min}$ and $SOC_{\max}$ denote the lower and upper limit of the battery bank, respectively, $P_{ch}^{\max}$ and $P_{dis}^{\max}$ indicate the maximum charging and discharging power of the battery (W), respectively.

Besides, the hydrogen storage is constrained based on its minimum and maximum capacity given by:

$$C_{H_2}^{\min} \le C_{H_2}(t) \le C_{H_2}^{\max} \quad (4.47)$$

where $C_{H_2}^{\min}$ and $C_{H_2}^{\max}$ are the minimum and maximum levels of hydrogen in the storage tank, respectively.

4.9.2 Implementation of Non-dominated Sorted Genetic Algorithm (NSGA-II)

The optimization simulations are developed in the Matlab environment. NSGA-II, which is a powerful multiobjective evolutionary algorithm based on Pareto-optimal solutions, is utilized to find the optimal system configuration [104]. A fast non-dominated sorting technique is employed in NSGA-II to sort the population into various non-dominated levels, with each solution being assigned fitness, which is equal to its non-dominated level [105]. This technique, together with elitist strategy, could provide a better spread of solutions, fast convergence towards the Pareto-optimal front, and preserve the solution diversity [106]. The obtained Pareto-optimal solutions in this algorithm comprise a set of optimal solutions called the Pareto front.

The basic steps illustrated in Fig. 4.1 for solving nonlinear optimal configuration of the system are presented as follows:

Step 1: Input the primary data, such as annual meteorological data of the investigated location (hourly solar radiation, ambient temperature, and wind speed), technical as well as economic data for components in the system, emission parameters, biophysical parameters of the cultured pond, and parameters of NSGA-II algorithm.

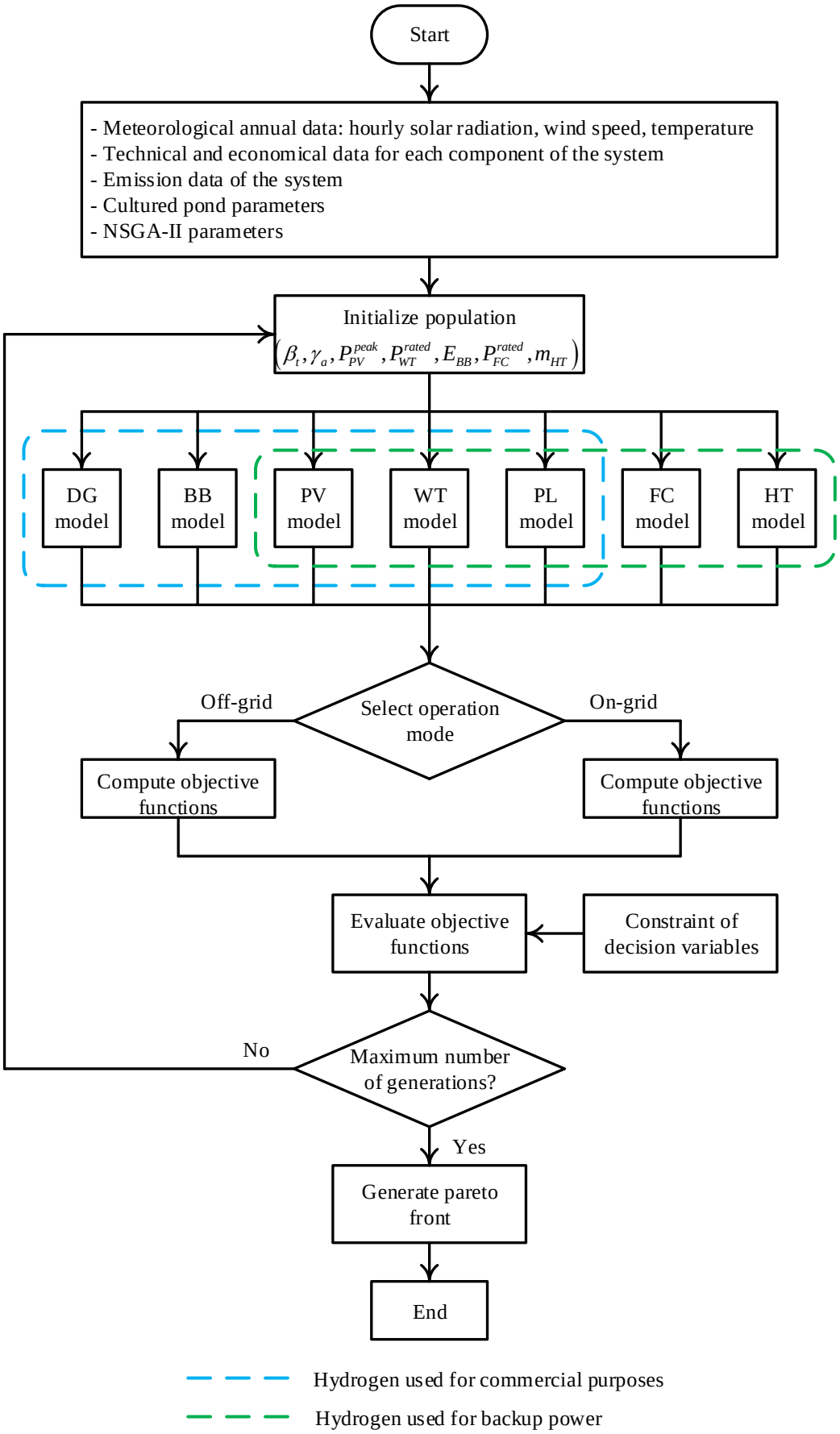

Figure 4.1 Flowchart of NSGA-II for optimization under multiobjective functions.

Step 2: Produce the initial population based on decision variables (azimuth angle, tilt angle, the capacity of PV, wind turbine, battery, fuel cell, and hydrogen tank), which are gene codes of each individual in the population with size N_{pop}. Then apply genetic manipulation, such as crossover and mutation mechanisms, to produce the offspring population.

Step 3: Compute the energy output for a one-year operation through the combination between the input data and such system models as PV, wind turbine, battery, diesel generator, fuel cell, hydrogen tank, and power load.

Step 4: Select the operation modes and calculate the objective functions according to the various system configurations in which the by-product hydrogen is used for commercial purposes or stored for backup power.

Step 5: Implement NSGA-II to assess objectives according to objective functions and constraints.

Step 6: Update the initial population and repeat step 2 if the maximum number of iterations is not satisfied.

Step 7: Sort obtained solutions and generate Pareto set for sorted non-dominated solutions when the termination criteria are met.

The population size and the number of generations of the algorithm are set as 200. Furthermore, the crossover and mutation rates of decision variables are set as 0.9 and 0.1, respectively.

4.10 Sensitivity Analysis for Sustainable Hybrid Energy Systems

4.10.1 The External Uncertainty Models

The meteorological factors, such as solar irradiance, ambient temperature, and wind speed, are sensitive to a particular topography due to their intermittent nature. As a result, the generated power from such renewable energy resources as solar and wind power is variable and uncertain; however, these power resources have stochastic behavior, which could be characterized by a probabilistic distribution function (PDF). Furthermore, to evaluate the influence degree of the interannual variations of meteorological variables on optimization outcomes, the sensitivity analysis is conducted by Monte Carlo simulation based on scenarios including the uncertainties.

The stochastic uncertainty model representing the deviations from the original series follows the PDFs. The interannual variations of average daily irradiation, average temperature, and average wind speed of a whole year are described by a Gaussian PDF with mean value and standard deviation [107].

The uncertain scenarios having hourly series of meteorological variables in a year are generated according to random samples following the Gaussian distribution, the hourly values of each original series, and the annual mean values of the uncertain variables in several years, as shown in the following equation [107]:

$$\theta_j(t) = \varphi_j(t) \cdot \frac{\mathcal{N}_k\left(\mu_j, \sigma_j^2\right)}{\mu_j} \qquad \left(1 \le k \le N_{samp}\right) \tag{4.48}$$

where $\theta_j(t)$ is the uncertain parameters, $\varphi_j(t)$ denotes such time-dependent phenomena as solar irradiance ($j = G$), air temperature ($j = T_a$), and wind speed ($j = v$), and N_{samp} is the number of discrete samples followed by a Gaussian PDF $\mathcal{N}\left(\mu, \sigma^2\right)$ with annual mean and standard deviation.

4.10.2 Sensitivity Analysis by Monte Carlo Simulation

It is necessary to carry out sensitivity analysis for optimization outcomes due to uncertainties in input variables. Nonetheless, the Monte Carlo analysis method, which often applies to assumptions for system cost, is useful when the input values are exposed to uncertainties [108]. Hence, Monte Carlo simulation is conducted since it is the most suitable method for complicated systems having a lot of uncertainties [109].

To evaluate the effect of uncertain parameters on the fitness of the system, the procedures of sensitivity analysis by Monte Carlo simulation after performing deterministic optimization in Fig. 4.2 are shown below:

Step 1: Collect data of the system for Monte Carlo simulation.

Step 2: Perform statistical analysis from historical and given data to obtain mean values, standard deviations for several years.

Step 3: Generate uncertainty scenarios with a total of N_{samp} random samples from Gaussian PDFs.

Step 4: Calculate the output power for a one-year operation by combining the generated scenarios and optimized decision variables through system models.

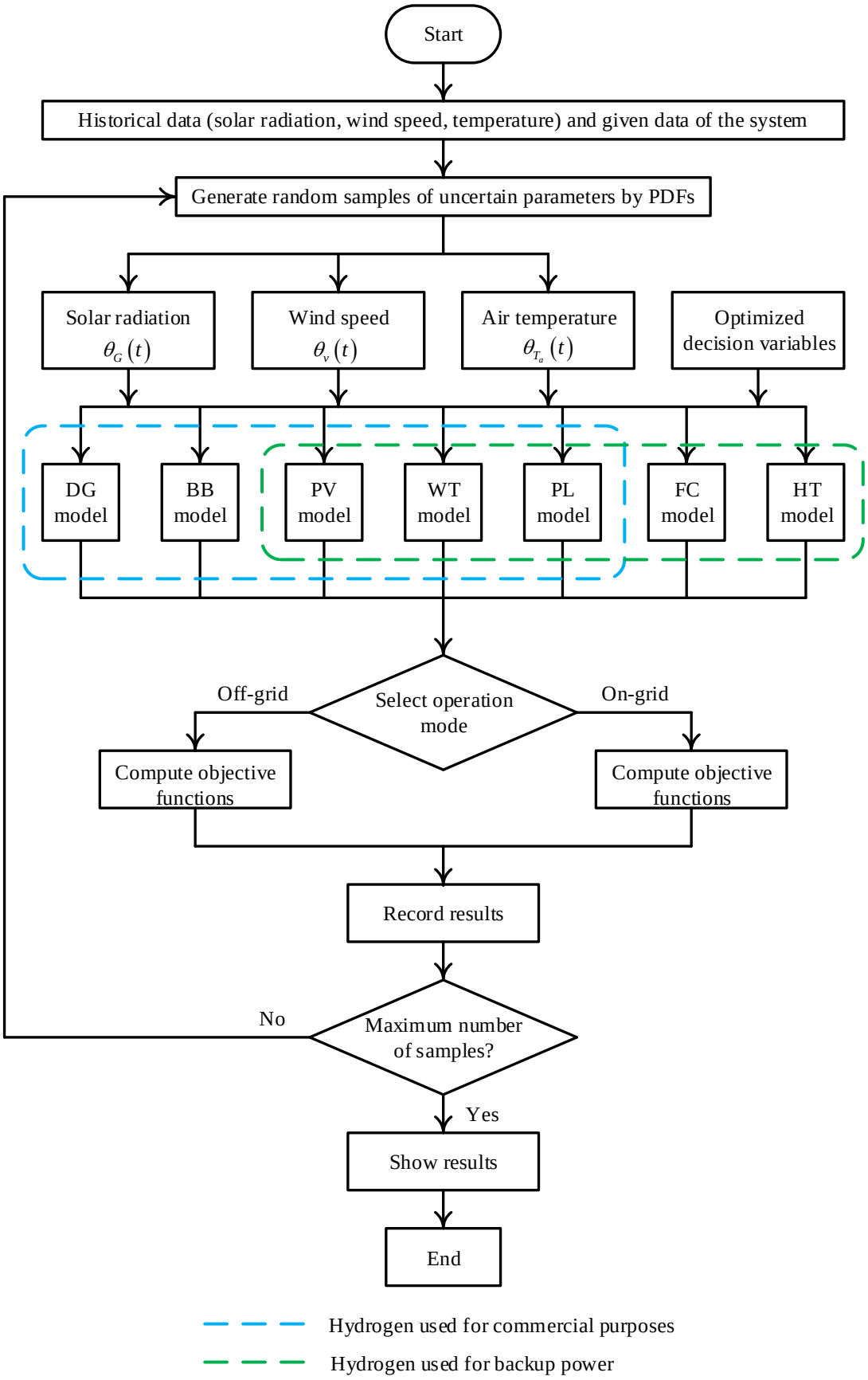

Figure 4.2 Framework of scenario development by Monte Carlo simulation for sensitivity analysis.

Step 5: Select the operation modes and compute the fitness corresponding to each mode.

Step 6: Keep recording results and repeat step 3 if the maximal number of iterations is not reached.

Step 7: Extract results for sensitivity analysis when the stopping criteria are met.

5. Analysis of Sustainable Hybrid Energy Systems for Shrimp Farms

5.1 Case Study

5.1.1 Case Data Introduction

The proposed energy system and its optimal design are applied to a shrimp farm located at Vinh Chau, Soc Trang province, which is situated 9.42° north latitude, 106.7° east longitude, GMT+7 time zone, and -8 m elevation. This province is one of the large shrimp producers in the Mekong Delta, Vietnam.

The investigated shrimp farm illustrated in Fig. 5.1 consists of three grow-out ponds, one pond for storing water, and another pond for water treatment. Each grow-out pond is of a depth of 1.2 m and a surface area of 1400 m^2. The PV panels are mounted above these ponds, with the appropriate spacing between each panel.

Figure 5.1 Ponds at the investigated shrimp farm.

The location of the shrimp farm has, in general, a tropical climate divided into dry and rainy seasons with the former starting from November to April and the latter lasting from May to October. The meteorological data, which includes solar irradiance, air temperature, and wind velocity captured by a sample per hour precision in a typical year, is shown in Fig. 5.2. The solar irradiance is somewhat constant during the year with a daily mean value of 4.8 kWh/m^2 [110]. The average value of the air temperature is about 27 °C. Moreover, the wind speed in this region is abundant at 80 m height, with its value averaging at 7 m/s [111].

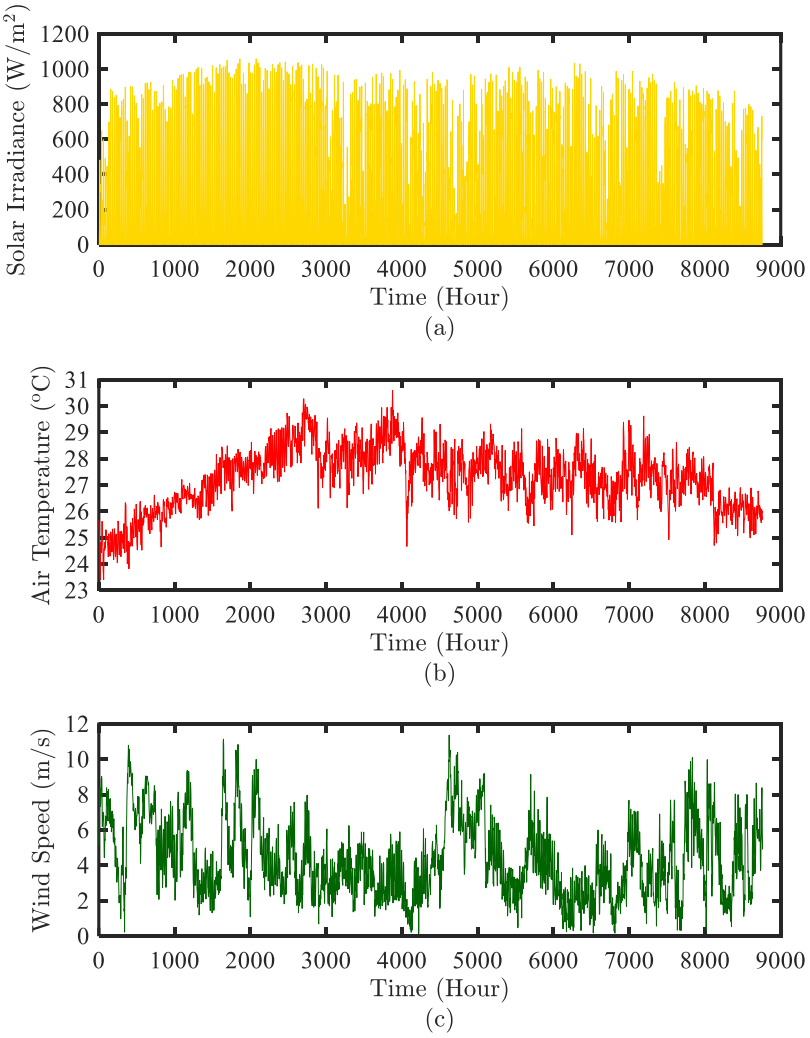

Figure 5.2 Annual solar irradiance (a), air temperature (b), and wind speed at 10 m height (c).

The rearing period of shrimp at the implemented farm lasts about three months. The primary power at the farm during the cultivating period is consumed by the electrolyzer, which is employed to produce pure oxygen for aerating cultured ponds, at 80%, leaving the baseload at 20%.

Table 5.1 Biophysical characteristics of grow-out ponds

Quantity	Value	Refs
Number of ponds	3	
Surface area of grow-out pond (m^2)	1400	
Depth of water (m)	1.2	
Salinity (ppt)	1	
Average water temperature (°C)	30	
Air pressure (atm)	1	
Average shrimp weight (g)	30	
Stocking density (shrimp/m^2)	200	
Average water respiration rate ($mgL^{-1}h^{-1}$)	0.4	[81]
Average sediment respiration rate ($mgL^{-1}h^{-1}$)	0.43	[81]
Oxygen absorption efficiency of bubble system (%)	95	[72]
Ratio of PAR to broadband solar radiation (m^2/W)	0.02	[80]
Average chlorophyll-a concentration (mg/L)	0.1	[112]

The total oxygen requirement in grow-out ponds, which have biophysical characteristics presented in Table 5.1, determines operation modes of the electrolyzer. The power consumption of electrolyzer changes during the day according to losses of oxygen due to the respiration of organisms in ponds and oxygen production by photosynthesis, shown in Fig. 5.3. The electrolyzer consumes the highest amount of energy at night due to the decline in photosynthetic oxygen generation by phytoplankton.

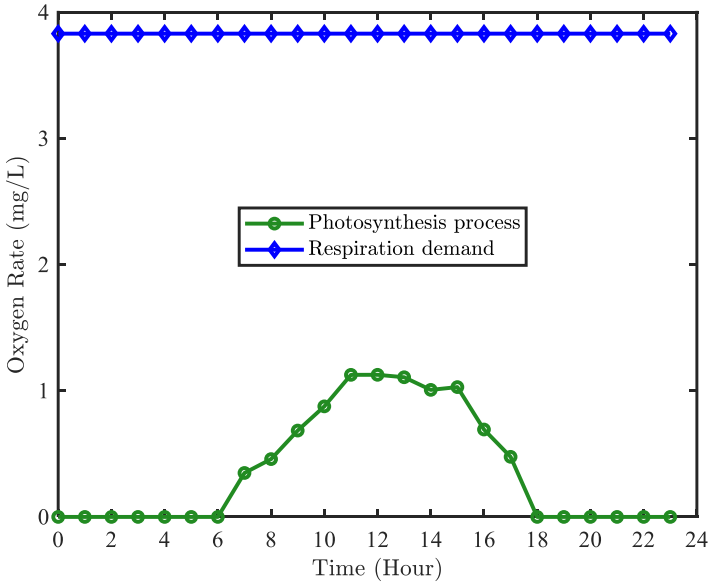

Figure 5.3 Hourly oxygen rate by photosynthesis process and respiration demand.

It can be seen from Fig. 5.4 that the overall system requires more power at night. In addition, the load profile of the system is constituted by a significantly high amount of energy from the electrolyzer. At the same time, the baseload requires a small

amount of power from the system. Thus, the load profile of the system, followed by the pattern of the electrolyzer, demands more electricity at night.

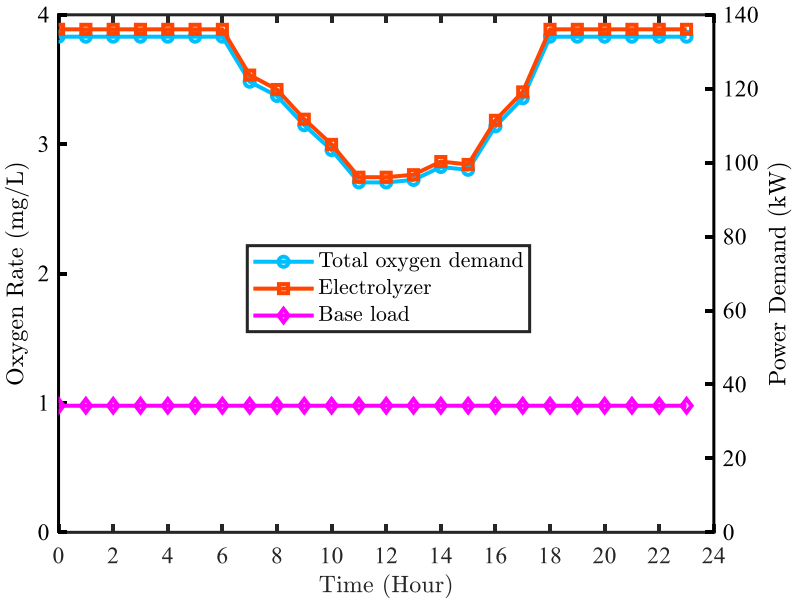

Figure 5.4 Hourly oxygen requirement and power demand at the shrimp farm.

5.1.2 Parameter Settings

The specifications of components in the system at the shrimp farm for techno-economic optimization are described in Table 5.2. The project lifetime of the system is assumed to be 20 years based on the longest lifespan of the component in the system.

Table 5.2 Parameter settings for simulation optimization

Quantity	Value	Refs
Initial cost of PV ($/kW)	1000	[113]
Initial cost of wind turbine ($/kW)	1980	[113]
Initial cost of electrolyzer ($/kW)	1200	[114]
Initial cost of fuel cell ($/kW)	3000	[115]
Initial cost of hydrogen tank ($/kg)	1000	[116]
Initial cost of battery ($/kWh)	400	[117]
Initial cost of inverter ($/kW)	90	[118]
Initial cost of diesel generator ($/kW)	336	[119]
Initial cost of mechanical aerator ($/kW)	440	[88]
Cost of diesel fuel ($/L)	0.9	
Purchase price of electricity from grid ($/kWh)	0.0804	
Sale price of electricity to grid ($/kWh)	0.0935	[120]
Sale price of hydrogen ($/kg)	2	[121]
Project lifetime (years)	20	
PV system lifetime (years)	20	[122]
Wind turbine system lifetime (years)	20	[123]
Electrolyzer lifetime (years)	10	[114]
Fuel cell lifetime (years)	5	[115]
Hydrogen tank lifetime (years)	20	[116]
Battery lifetime (years)	12	[117]
Inverter lifetime (years)	15	[119]
Diesel generator lifetime (years)	7	[119]
Mechanical aerator lifetime (years)	4	[88]
Tax rate (%)	10	[124]
Interest rate (%)	6	[124]
Maintenance rate of PV (%)	1.5	[113]
Maintenance rate of wind turbine (%)	1.8	[113]
Maintenance rate of electrolyzer (%)	2.5	[114]
Maintenance rate of fuel cell (%)	5.8	[115]
Maintenance rate of hydrogen tank (%)	1	[116]
Maintenance rate of battery (%)	4	[117]
Maintenance rate of diesel generator (%)	2	[125]
Maintenance rate of mechanical aerators (%)	10	[88]

5.2 Hydrogen Used for Commercial Purposes

5.2.1 Scenarios for Simulation Optimization

Three scenarios are conducted in the islanded operation mode for simulation optimization, as illustrated in Table 5.3. Scenario S1, which is the combination of PV and battery with a diesel generator as backup power, is analyzed at the shrimp farm. Scenario S2 considers the integration of wind turbines, battery bank, and a diesel generator. The hybrid energy system in scenario S3 comprises of PV, wind turbines, and battery with the support of backup power from a diesel generator in which the capacity of each component is optimized to satisfy the power demand at the farm. The best configuration of components in the system in one of the concerned scenarios is

implemented in the grid-connected mode in which the backup power is replaced by the national grid instead of the battery as well as the diesel generator. Furthermore, the surplus power in the on-grid operation mode is sold to the national network according to the FIT policy.

Table 5.3 Summary of simulated scenarios

Description	Scenario S1	Scenario S2	Scenario S3
PV	x	-	x
Wind turbine	-	x	x
Battery	x	x	x

5.2.2 Optimization Results in Stand-Alone Mode for Scenario S1

The Pareto front, which is shown in Figure. 5.5, indicates the relationship between *ACS* and *EMI* for the system involving PV arrays, the battery bank, and a diesel generator.

It can be seen from Fig. 5.5 that the amount of CO_2 emission is significantly high, with the level being more than 30 tCO_2 when the *ACS* of the system is lower than 360,000 USD. The value of *EMI* decreases considerably with the increase of *ACS* from 340,000 USD to 360,000 USD. Afterward, the amount of CO_2 emission declines fractionally with the increment of the *ACS*, reaching 14.05 tCO_2 with the maximal value of *ACS* at 581,000 USD.

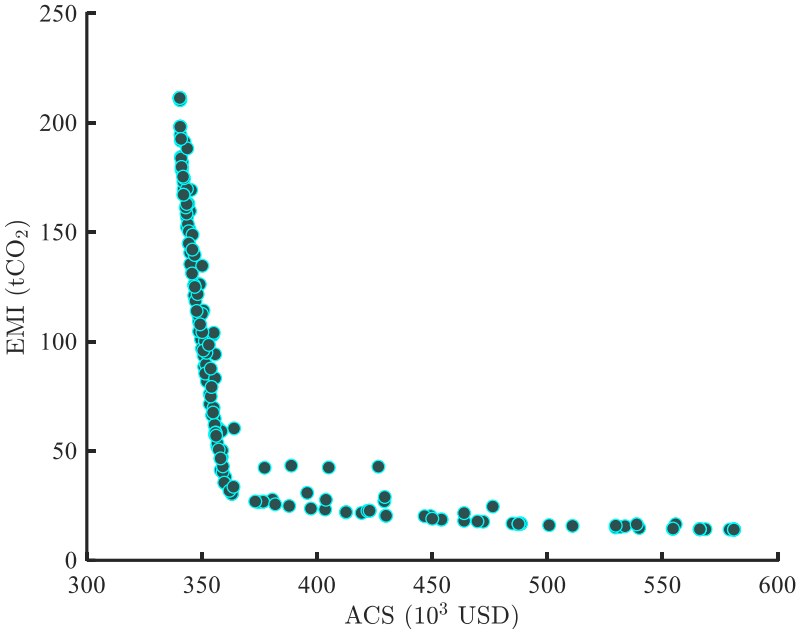

Figure 5.5 Pareto front for scenario S1.

Moreover, the process of the simulation optimization for scenario S1 is clarified specifically by dissecting the relationship between the capacity of PV and battery with

CO_2 emission, presented in Fig. 5.6. The capacity of the battery is affected by the capacity of the PV system. The low capacity of the PV system often coincides with the small capacity of the battery. In combination, negative impacts on the environment are inevitable due to the high amount of CO_2 emission released from the operation of the diesel generator to meet the power shortage. The amount of CO_2 emission of the system, nonetheless, declines with the increase in capacity of PV and the battery bank, which results in a decrease in the backup power from the diesel generator. Furthermore, the battery capacity cannot rise beyond 6 MWh because the PV peak capacity reaches the maximum available values (1,000 kW_p).

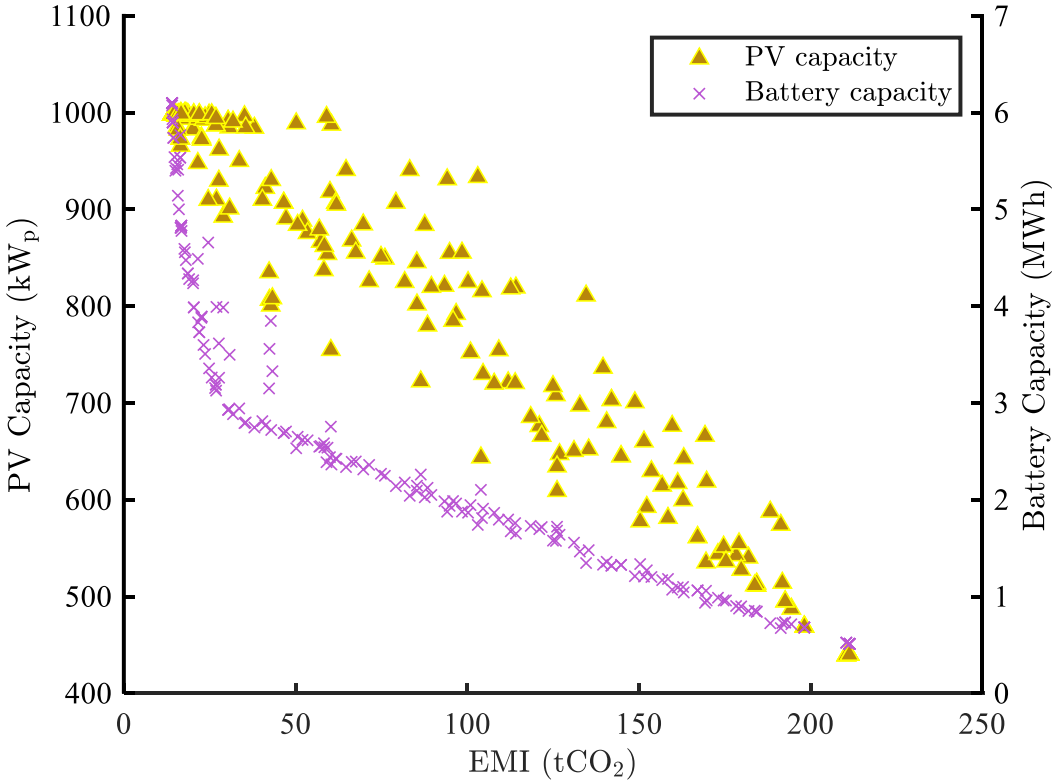

Figure 5.6 The relationship between PV and battery capacity with emission.

5.2.3 Optimization Results in Stand-Alone Mode for Scenario S2

It can be seen from the Pareto front of scenario S2 depicted in Fig 5.7 that the increase in the system cost leads to a dramatic decline in CO_2 emission, reaching the minimum value at 72.67 tCO_2 with the system cost at 1,032,000 USD.

As shown in Fig. 5.8, the values of CO_2 emission of the system initially decrease due to the increase in capacity of the WT systems until 120 tCO_2. Afterward, the CO_2 emission declines further by increasing the capacity of the battery, which closes to the upper boundary of 10 MWh as the wind turbines reach the maximal capacity. Although the WT system capacity closes to the upper limit of 1,000 kW_r, the amount of CO_2

remains substantially high, which is caused by diesel generator to satisfy the power deficit of the system.

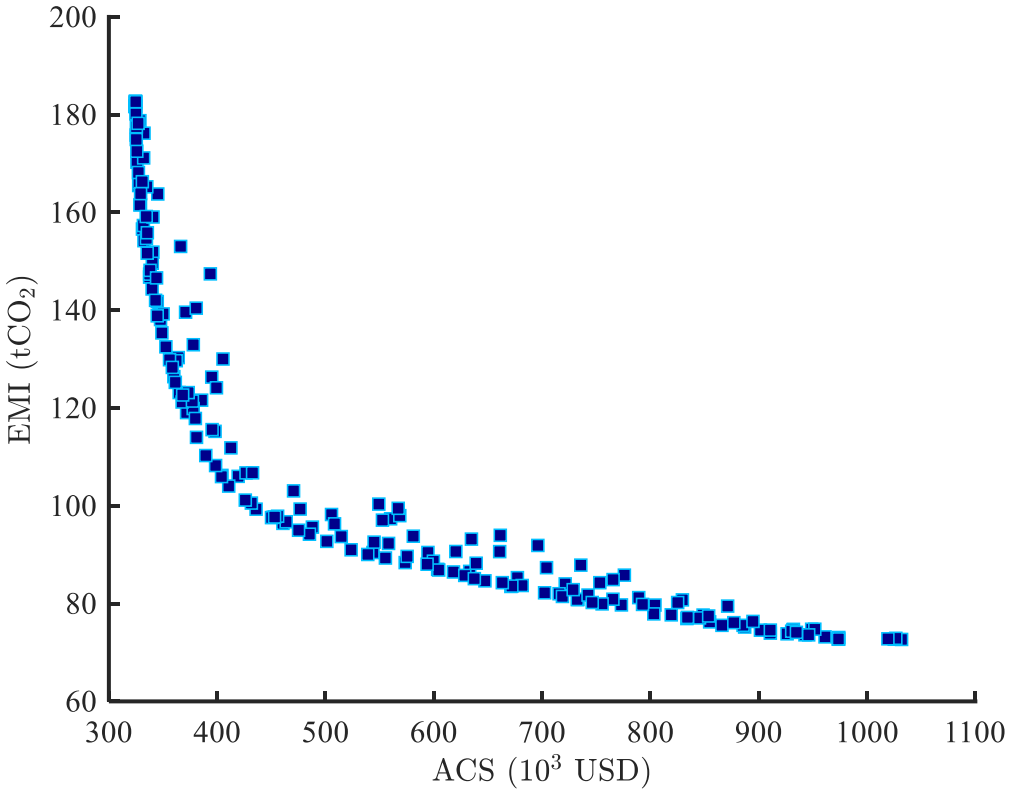

Figure 5.7 Pareto front for scenario S2.

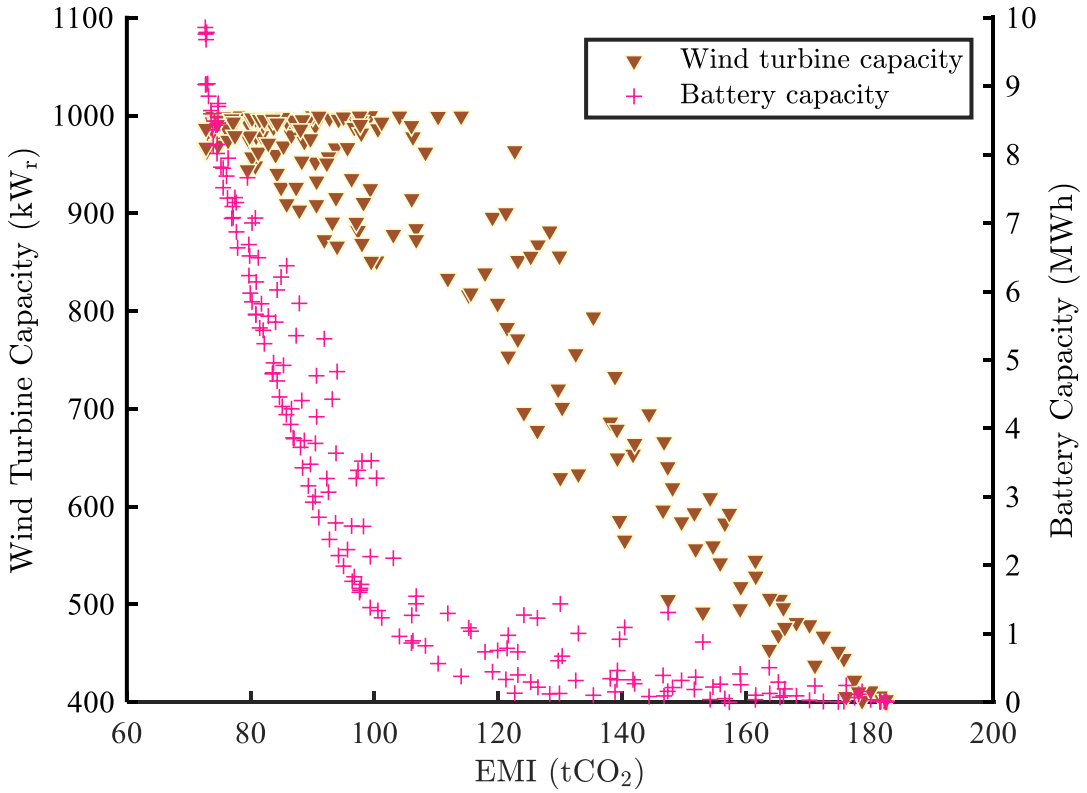

Figure 5.8 The relationship between wind turbine and battery capacity with emission.

The system in scenario 2 has significantly high *ACS* as well as *EMI* due to the high capital cost of wind turbines and moderate wind speed at the investigated shrimp farm in which wind turbines could not produce efficient power for the system. As a result, the system requires more capacity of the battery for storage and fulfills power shortage from the diesel generator.

5.2.4 Optimization Results in Stand-Alone Mode for Scenario S3

Scenario 3 combining power resources between PV and wind power with the support of battery storage and a diesel generator is of a similar trend to scenario S1 and S2.

As can be seen in Fig. 5.9, the increase in the system cost results in decline in greenhouse gas emissions. The system stops releasing CO_2 when its cost reaches the maximum value of 794,000 USD.

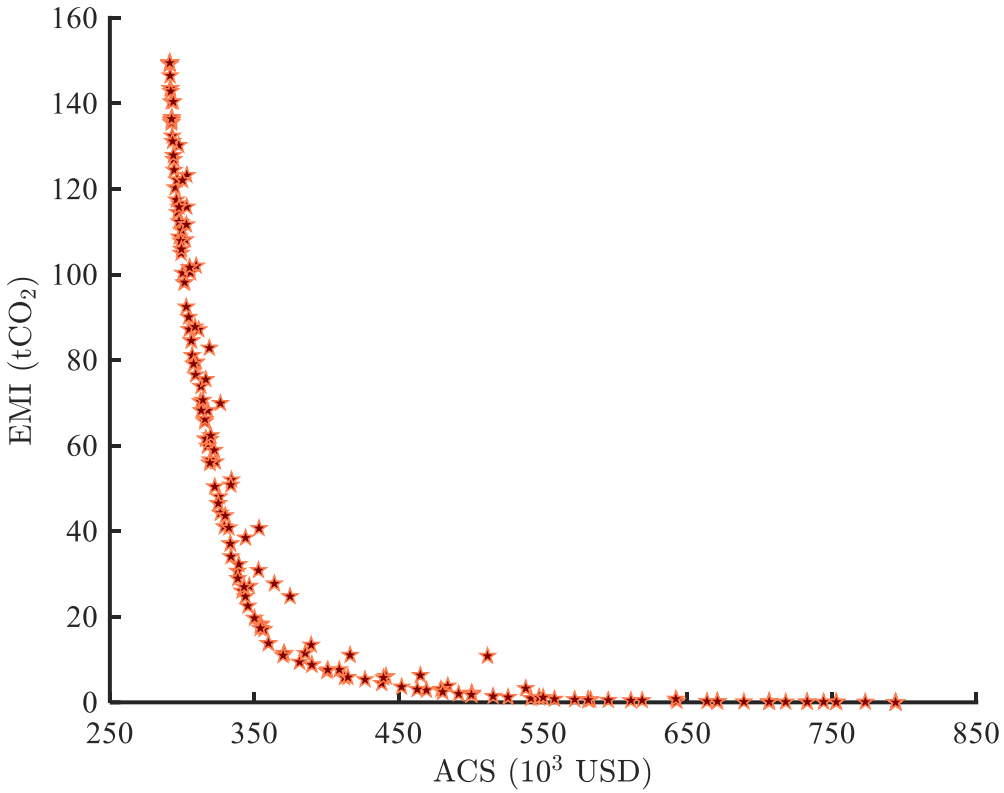

Figure 5.9 Pareto front for scenario S3.

In comparison with scenarios S1 and S2, the values of minimal *ACS* and *EMI* in scenario S3 are the lowest, as illustrated in Table 5.4 since the combination between PV and wind power could not only satisfy the power load but also lead to a decrease in battery capacity and power requirement from the diesel generator, resulting in the decline in the overall capital cost of the system and CO_2 emission. In autonomous

operation modes, the minimum value of *ACS* of S3 is the lowest, at about 291,444 USD. On the contrary, the *ACS* of S1 is the highest, which is higher than that of S2 at 15,940 USD. Regarding the emission of the system corresponding to ACS_{min}, scenario S1 releases the highest amount CO_2, at about 211.34 tCO_2, which is much higher than S2 (181.67 tCO_2). Scenario S3 has the lowest level of emissions at 149.14 tCO_2.

Table 5.4 Optimization results corresponding with the minimum annualized cost of system for each scenario.

Description	Scenario S1	Scenario S2	Scenario S3
PV capacity (kW_p)	439.76	-	255.09
Wind turbine capacity (kW_r)	-	406.39	260.6
Battery capacity (kWh)	511.66	13.19	274.74
ACS_{min} (USD)	340,364	324,424	291,444
EMI (tCO_2)	211.34	181.67	149.14

Among three scenarios implemented for simulation optimization in the off-grid operation mode of the system, scenario S3 is considered the best configuration for the investigated shrimp farm, integrated by between PV panels and wind turbines with the support of battery and diesel generator. The integration of components in scenarios S3 could power the system satisfactorily with the lowest CO_2 emission and the most competitive annualized cost of the system. Hence, the configuration of PV arrays and wind turbines is chosen for simulation optimization in grid-connected operation mode.

5.2.5 Optimization Results in Grid-Connected Mode

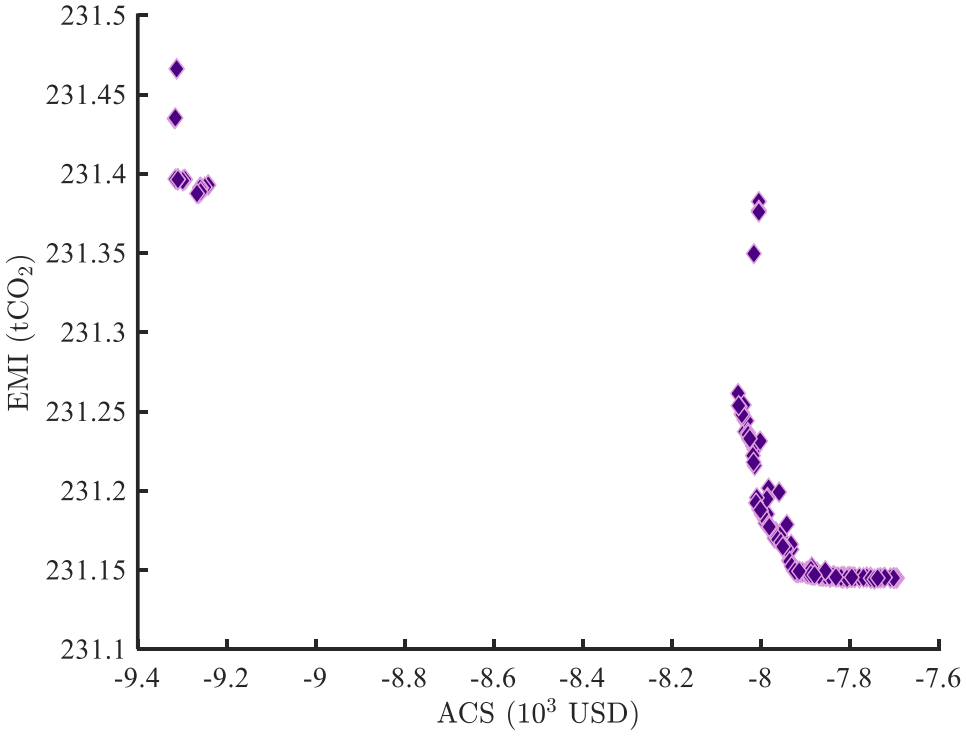

Figure 5.10 Pareto front for on-grid mode.

The Pareto front in a grid-connected operation mode in which the backup power is totally supplied by the national grid instead of battery storage and a diesel generator is presented in Fig. 5.10. It can be seen that the *ACS* has negative values, which means that the system could produce revenues by selling not only by-product hydrogen but also the surplus electricity to the national network.

Table 5.5 provides a comparison among islanded mode, grid-connected mode, and conventional aeration system (CAS) powered by the national network. As shown in Table 5.5, when the project lifetime is over, the grid-connected system could realize the minimum cost at about -7,694 USD from selling the surplus electricity together with hydrogen. The *ACS* of scenario S3 is about eight times higher than that of the CAS (291,444 USD and 35,090 USD, respectively). In addition, the islanded system could only produce profits from selling hydrogen while the excess energy is stored in the battery to supply power for the system anytime when renewable power is not available. Besides, the initial capital cost of the battery is not only high, but it has to be replaced one time over the lifetime period, according to Table 5.2, resulting in additional cost in the overall expense of the system.

When the CO_2 emission is considered, the off-grid system S3 releases the lowest amount of gas emissions, at 149.14 tCO_2, which is dramatically lower than grid-connected mode and the CAS, with the former having a slightly lower level than the latter (231.14 tCO_2 and 261.96 tCO_2, respectively) as the advanced aeration system consumes considerably high power at night.

Table 5.5 Comparison between scenario S3, on-grid mode and conventional aeration system.

Description	Scenario S3	On-grid mode	CAS
PV capacity (kW_p)	255.09	992.59	-
Wind turbine capacity (kW_r)	260.6	998.10	-
Battery capacity (kWh)	274.74	-	-
ACS (USD)	291,444	-7,694	35,090
EMI (tCO_2)	149.14	231.14	261.96

5.3 Hydrogen Used for Backup Power

5.3.1 Optimization Results in Stand-Alone Mode

The relationship between *LPSP* and *ACS* in stand-alone operation mode, which is powered by PV arrays and WT with and without energy storage, is depicted in Fig. 5.11. This figure presents the annualized cost of the system at various reliability levels.

The *LPSP* value decreases with the rise of *ACS*. The lowest value of *LPSP* is 0 indicating the highest reliability whilst the value of 1 shows that the load demand is never satisfied.

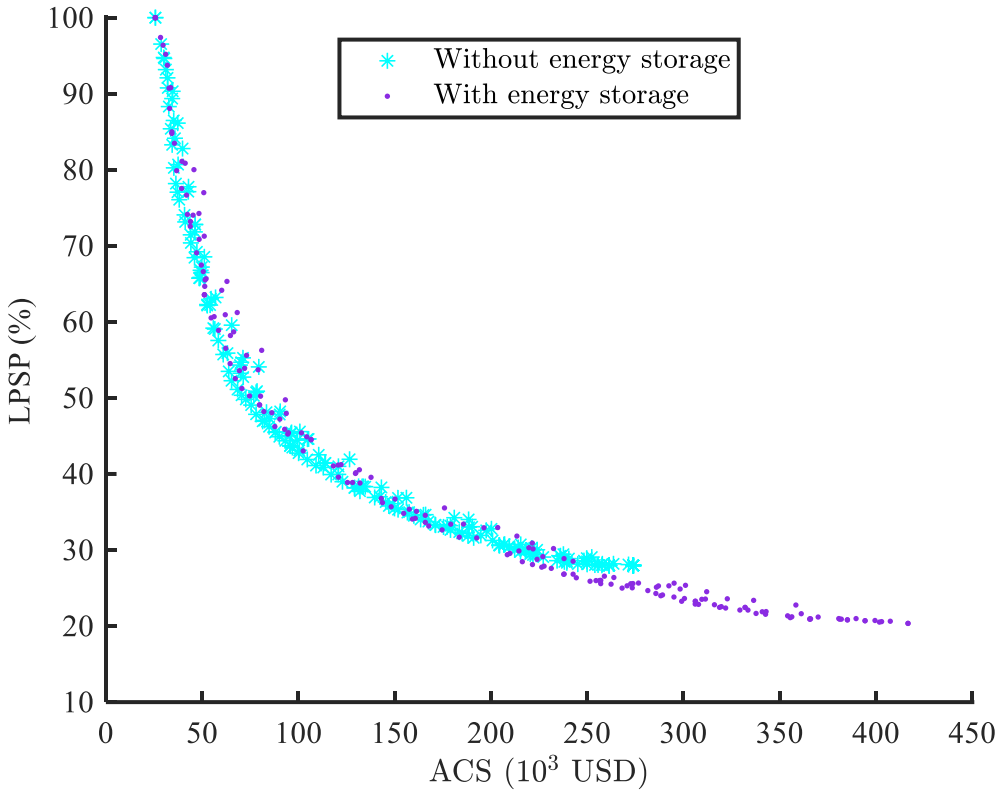

Figure 5.11 Pareto fronts in stand-alone mode.

As shown in Fig. 5.11, the system without energy storage has the minimum value of *LPSP* at about 28%, while this value of the system supported by energy storage is at about 20%. On the one hand, the reliability of the system supported by energy storage, i.e., fuel cell and hydrogen storage, is improved slightly, at about 8% due to the low efficiency of the fuel cell. The reason for this is that the hydrogen fuel, which is directly converted into electricity by fuel cell for backup power, is the by-product through water electrolysis. Apart from that, the production flow rate of hydrogen depends on the operation of the electrolyzer, which is used to produce the main-product oxygen according to DO changes in cultured ponds to provide aeration for cultivated species. On the other hand, the system cost corresponding to $LPSP_{min}$ (20 %) is about 416,620 USD, which is considerably higher than the system without energy storage (273,933 USD) due to the additional expense of the energy storage system.

Moreover, the process of simulation optimization is explained specifically by analyzing the relationship between the available capacity of power resources and *LPSP*, as shown in Fig. 5.12. The rise in the capacity of PV and WT systems

significantly improves the reliability of the system. However, when the value of *LPSP* is lower than 30%, *LPSP* decreases fractionally since the capacity of PV and WT systems approach their limit. The maximum available value of WT is higher than that of PV (1,000 kW_r and 704 kW_p, respectively) because the system load demands more power at night than the daytime. In addition, the moderate wind velocity at the farm might not produce sufficient energy for the system at night; hence, the reliability of the system could not be improved dramatically even the wind turbine system reaches the maximal rated capacity.

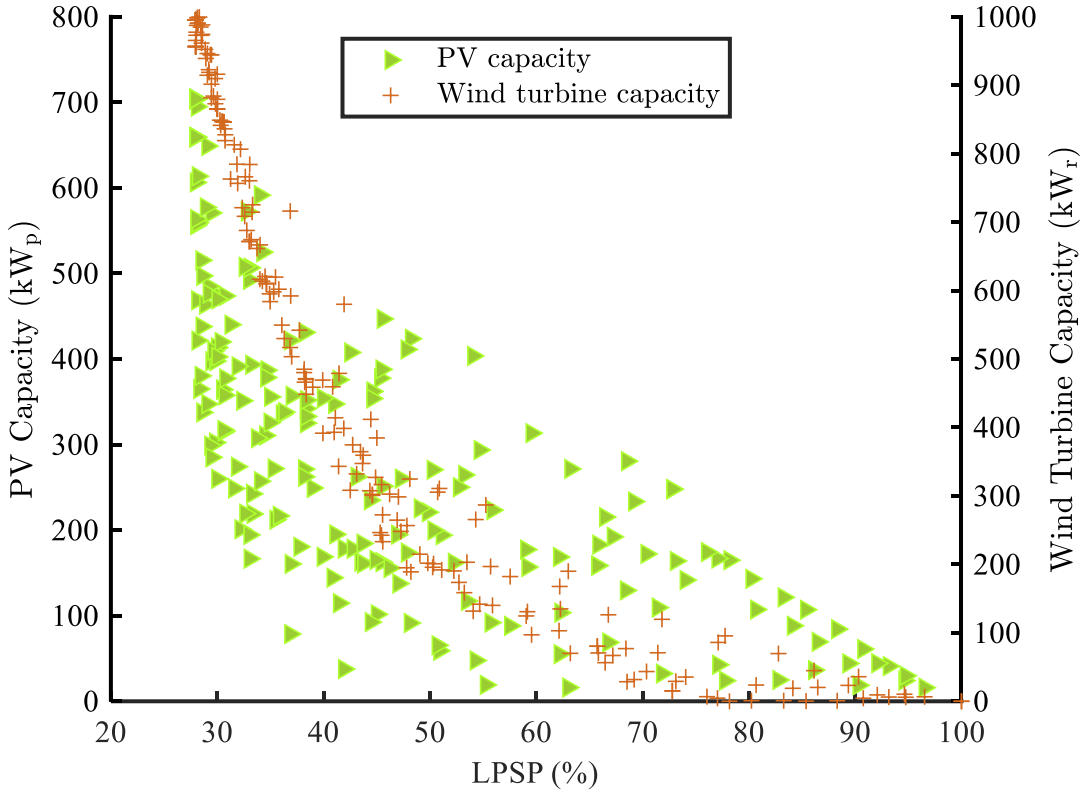

Figure 5.12 The relationship between the capacity of PV and WT with LPSP.

Similarly, the influence of FC capacity on values of *LPSP* and *ACS* is illustrated in Figure. 5.13. The utilization of FC to provide backup power generated from by-product hydrogen could improve the reliability of the hybrid system. It can be seen in Fig. 5.13 that the *LPSP* initially decreases dramatically, although the capacity of FC is still very small. The cause of this decline is the increase in the capacity of renewable energy resources. Nevertheless, when the renewable resources are close to their upper boundary, the value of *LPSP* continues to decline gradually with the sharp rise of FC capacity, reaching 20% with the maximal values of *ACS* and FC capacity at about 416,620 USD and 67 kW_r, respectively. The system cost witnesses a dramatic increase due to the high capital cost of FC and associated HT.

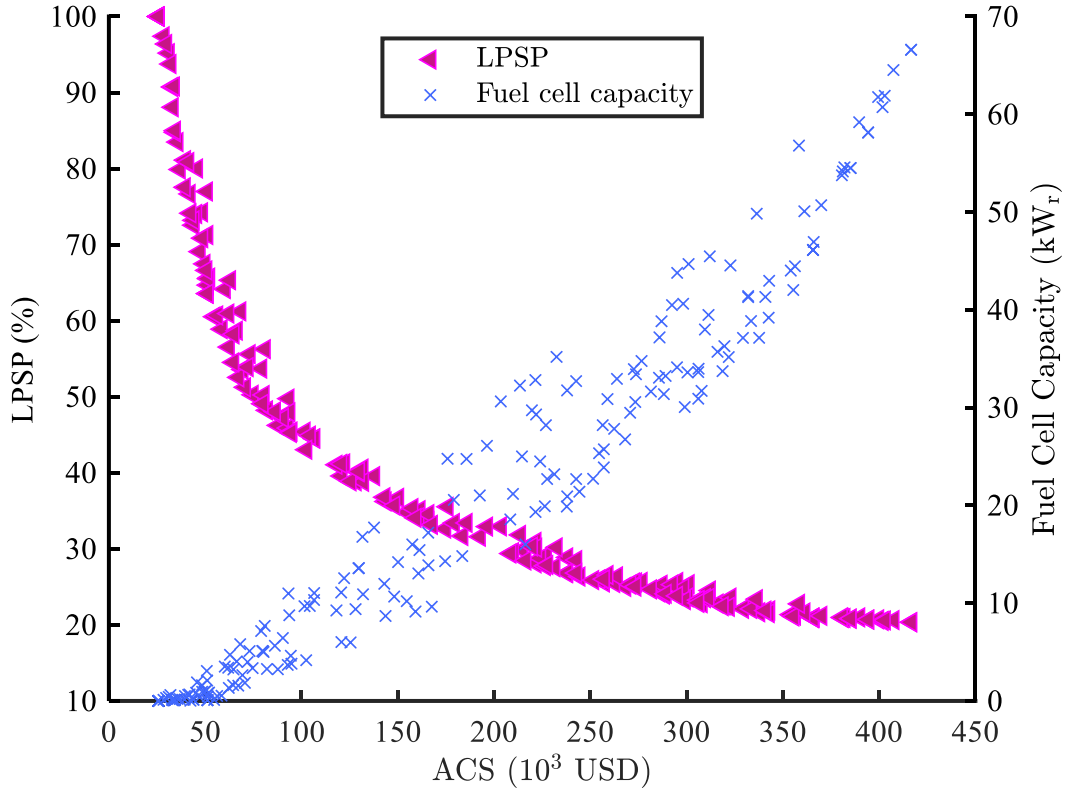

Figure 5.13 The relationship between FC capacity and LPSP with ACS.

Undoubtedly, the power system having the minimum value of *LPSP* at 20% could not meet the security of the aeration system. The aeration system for aquaculture industry necessitates stable, sufficient, and secure power resources, which could supply power continuously without lengthy blackout; therefore, the proposed aeration system energized by renewable resources and supported by FC as primary backup must be connected to the national power system to satisfy the power shortage.

5.3.2 Optimization Results in Grid-Connected Mode

When the proposed system operates in connection with the national power network, the carbon dioxide emission from the national grid is considered as the objective function *EMI* besides *ACS*. The Pareto front optimized in on-grid mode with the total support from the national grid as the secondary backup power system is presented in Fig. 5.14. The increase in the *ACS* leads to a significant decrease in CO_2 emission, reaching the minimal value at 124.32 tCO_2 with the *ASC* at 152,386 USD. Nevertheless, the *ACS* has negative values indicating that the proposed system is able to obtain revenues from selling surplus electric power to the national grid and dumped hydrogen to local fertilizer factories.

The optimal solutions from the Pareto front are divided into two groups. The group with orange solutions in Fig. 5.14 has *ACS* values lower than *ACS* of the conventional

aeration system (CAS) run by paddlewheel aerators. On the contrary, the *ACS* values of the group with purple solutions are higher than that of the CAS.

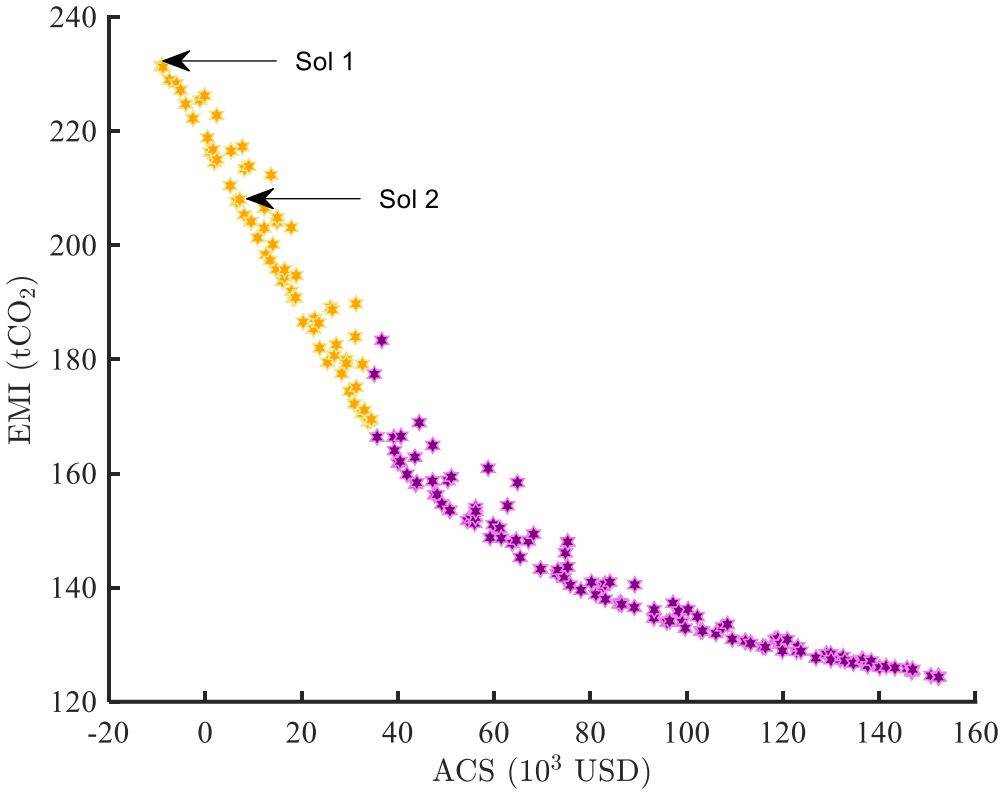

Figure 5.14 Pareto front for on-grid operation mode.

A comparison amongst two solutions of interest from orange solutions and the CAS powered by the national grid is illustrated in Table 5.6. Solution 1 (Sol 1) corresponds to the lowest value of *ACS* and the highest amount of CO_2 emission, while Sol 2 is the intermediate solution among orange solutions in Fig. 5.14. However, in a real application, designers could choose one of the orange solutions based on their preferences.

Table 5.6 Characteristics of two solutions of interest and conventional aeration system

Description	Sol 1	Sol 2	CAS
PV capacity (kW_p)	998.65	998.62	-
Wind turbine capacity (kW_r)	999.09	998.96	-
Fuel cell capacity (kW_r)	0.06	12.30	-
Hydrogen tank capacity (kg)	0.51	12.25	-
ACS (USD)	-9,112	7,160	35,090
EMI (tCO_2)	231.35	208.01	261.96

The capacity of PV and WT of Sol 1 reaches the maximum available values whilst the FC is not employed for backup power, which is totally purchased from the national network. Thus, besides selling surplus electric power to the national grid, all of the

dumped hydrogen from the electrolysis process is collected and sold to local fertilizer plants, producing revenues for farmers about 9,112 USD in a year. By contrast, the amount of emission released from the grid is high (231.35 tCO_2) compared to Sol 2 (208.01 tCO_2).

With the utilization of FC as backup power in Sol 2, the amount of CO_2 emission declines considerably in comparison with Sol 1 and the CAS (23.34 tCO2 and 53.95 tCO_2, respectively). The utilization of FC often coincides with HT. In combination, the extra cost associated with such configuration is inevitable. Although the cost of the system of Sol 2 is considerably higher than Sol 1, it is still significantly lower than the CAS (7,160 USD and 35,090 USD, respectively); hence, farmers could save about 27,930 USD per year.

5.4 Potential Carbon Tax and Sensitivity Analysis

5.4.1 Potential Carbon Tax Analysis

The potential carbon tax in case of hydrogen used for commercial purposes (scenario S3 and on-grid mode) and backup power (Sol 2) compared to the CAS is given in Table 5.7. Among scenarios, the on-grid mode is of the lowest potential carbon tax, at -1,388 USD/tCO_2. In contrast, the potential carbon tax of scenario S3 is the highest, at 2,272 USD/tCO_2. In other words, the most expensive technology to reduce CO_2 emission relative to the CAS is scenario S3, including the integration of renewable energy resources with the support of battery and diesel generator. The on-grid operation mode and Sol 2, whose backup power generated from by-product hydrogen and supported by the national grid, respectively, are cheap ways to reduce CO_2 emissions (-1,388 USD/tCO_2 and -518 USD/tCO_2, respectively).

Table 5.7 Potential carbon tax of scenarios compared to the CAS

Description	Scenario S3	On-grid mode	Sol 2	CAS
ACS (USD)	291,444	-7,694	7,160	35,090
EMI (tCO_2)	149.14	231.14	208.01	261.96
Potential carbon tax (USD/tCO_2)	2,272	-1,388	-518	Reference

In general, the on-grid mode and Sol 2 are economical solutions for shrimp production contexts in Vietnam.

5.4.2 Sensitivity of Deterministic Solutions

The simulation optimization showed that the proposed hybrid sustainable energy system, which could produce onsite pure oxygen for aerating shrimp ponds and use by-product hydrogen mainly either for commercial purposes or backup power, is a promising solution for shrimp aquaculture. Nonetheless, it is necessary to conduct sensitivity for these solutions due to uncertainties in the input variables.

The influence of uncertainties of the meteorological variables on optimal solutions is assessed by Monte Carlo simulation based on uncertain scenarios. A number of 1000 random samples are generated according to Gaussian PDFs for iteratively simulating the prosed system.

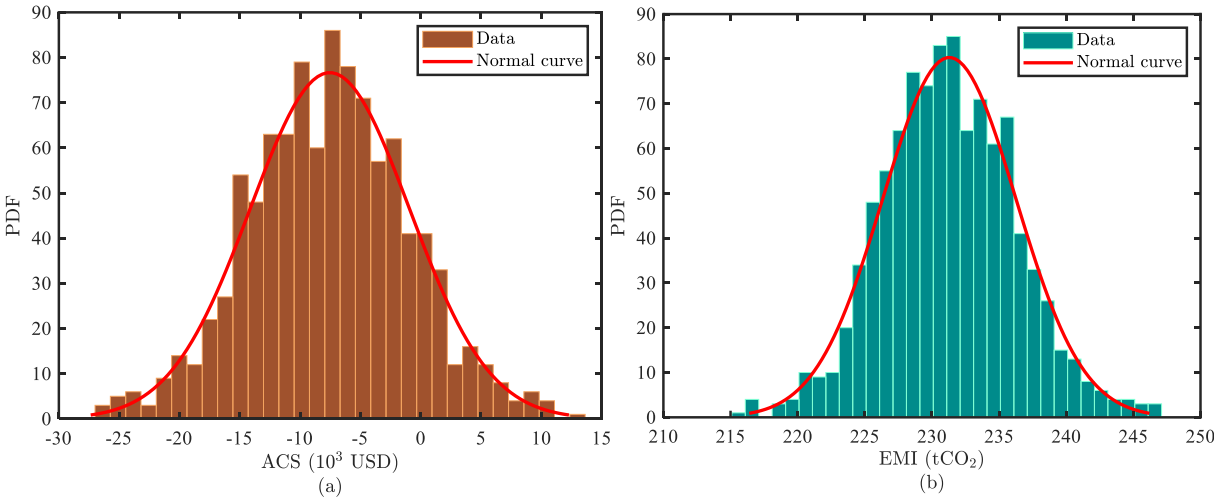

Figure 5.15 PDFs of the results of ACS (a) and EMI (b) for on-grid operation mode.

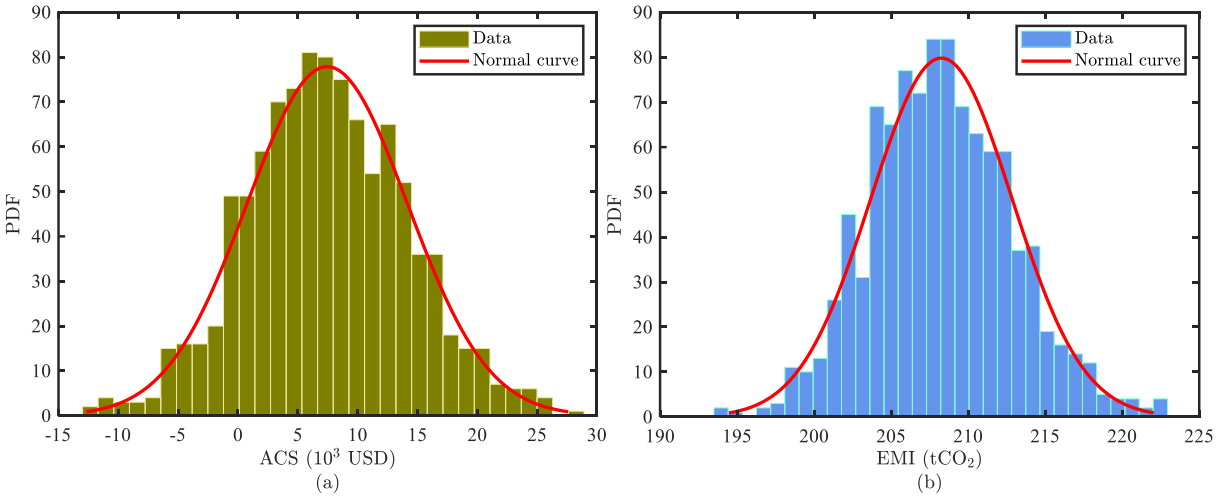

Figure 5.16 PDFs of the results of ACS (a) and EMI (b) for Sol 2.

The probabilistic simulation is performed over the on-grid operation mode and the intermediate Sol 2. The PDFs illustrated in Fig. 5.15 and 5.16 present the variability of

on-grid operation mode and Sol 2 with respect to the *ACS* and the *EMI*. The normal curves shown in Fig. 5.15 and 5.16 best fit the PDFs.

The average values, standard deviations, minimum, and maximum values of the *ACS* and the *EMI* are given in Table 5.8. The values of *ACS* of on-grid mode range between -26,859 USD and 13,571 USD, which means that farmers could get high revenues or pay less annual cost according to the uncertainties of meteorology. Sol 2 has values of *ACS* between -12,273 USD and 28,677 USD, which mean that farmers could get revenues or pay high annual cost according to the uncertainties of meteorology. Nonetheless, the maximum values of *ACS* with substantially low probability are lower than *ACS* of the CAS. Furthermore, the amount of CO_2 emissions of Sol 2 and on-grid mode fluctuates between 193.87 tCO_2 and 222.84 tCO_2, and from 215.87 tCO_2 to 246.99 tCO_2, respectively, which are significantly lower than *EMI* of the CAS.

Table 5.8 Results of sensitivity analysis for on-grid mode and Sol 2

Characteristics	On-grid mode		Sol 2	
	ACS (USD)	EMI (tCO_2)	ACS (USD)	EMI (tCO_2)
Mean	-7,531	231.29	7,457	208.26
Standard deviation	6,610	4.97	6,712	4.60
Min	-26,859	215.87	-12,273	193.87
Max	13,571	246.99	28,677	222.84

6. Conclusion and Future Works

6.1 Conclusion

Prioritizing the development of high technology with low carbon emissions, energy-saving, and sustainability is being encouraged in aquaculture in Vietnam, especially the shrimp industry. Therefore, an optimal design on a sustainable hybrid energy system for shrimp aquaculture is proposed in this dissertation. The designed system is quite different from current aeration systems for shrimp aquaculture in the configuration as well as operation.

In order to assess performance and validate the results of the proposed system, the simulation and optimization models were developed in the Matlab environment. Besides, the optimal results of the system were compared with the CAS run by paddlewheel aerators regarding technical, economic, and environmental aspects. An excellent avouchment found in optimal outcomes and sensitivity analysis shows that the proposed system connecting to the national grid in which the by-product hydrogen is primarily either sold for commercial purposes or used for backup power is the best solution instead of operating in islanded mode due to strictly-needed reliability. Moreover, when properly designed and operated, the system Sol 2 using electrolyzer energized by green energy resources to produce oxygen in situ for oxygenation based on the DO demand of shrimp and the by-product hydrogen through electrolysis process to generate backup power is the potential configuration in which the investigated shrimp farm could save a lot of energy and reduce environmental impacts. Likewise, the on-grid system in which the by-product hydrogen is sold for local fertilizer plants not only produces revenues but also is of low CO_2 emissions when the project is over.

In comparison with the CAS, the proposed system operating in such modes as on-grid and Sol 2 could achieve sustainable, economic, and environmental targets in which the Vietnamese government has declared its intension to encourage green energy development. In other words, farmers could save operation costs or even get revenues from reducing energy demand and contribute to environmental protection by limiting the release of CO_2 emissions for their aeration system in the shrimp aquaculture industry.

Last but not least, the breakthrough of the system is that new technologies have been applied, such as water electrolysis and hydrogen fuel cell in which both oxygen and hydrogen are utilized for the aquaculture sector. In the context of global development, the utilization of such technology might be suitable for intensive aquaculture, resulting in higher productivity as well as yields in a sustainable way. Although water electrolysis and hydrogen fuel cell technology are very expensive due to high investment costs, the technology is not mature and expected to progress. In the long run, the sustainable hybrid energy system, which is proposed in this dissertation, will be a breakthrough having a significant influence on the financial feasibility and environmental sustainability for the shrimp aquaculture industry. Moreover, the outcomes of this work can be guidelines to instruct optimal design and operation for aquaculture farms not only in Vietnam but also in countries around the world.

6.2 Future works

The simulation and optimization models were developed and implemented for a real shrimp farm context. The optimal results and their sensitivity analysis show that the proposed system satisfied the intended goal of showing the benefits and concepts, which are dominant in the conventional aeration system in terms of technical, economic, and environmental aspects. Nevertheless, there are many perspectives that should be improved.

The DO model implemented in this work is simplified due to its complexity. The respiration rates of shrimp, sediment, and water were assumed constant during the rearing period. However, the DO respiration rates of the pond vary continuously and depend on diurnal and nocturnal activities of organisms in the pond and many ambient factors. Therefore, it is necessary to modify and improve the current DO model into the dynamic model, which is capable of monitoring temporal and spatial changes of DO. In addition, the dynamic model of DO makes it possible for further studies on optimizing the size of components in the system, especially the capacity of the electrolyzer, and controlling operation of the system.

Besides the DO model, the other models should be validated by real-time simulation. Furthermore, the sizing method by stochastic simulation-based multiobjective optimization approach under real operating conditions would be applied to fulfill both optimality and robustness.

Further validation and experiment will make it possible for an accurate assessment of the proposed system regarding technical, economic, and sustainable points of view. The costs of components in the system were based on past research. The local costs of components, however, may be different. Thus, the survey on implemented sites should be conducted for future work. Moreover, stakeholders should work together to perform a long-term study on sustainable management for shrimp farms to save energy costs and reduce environmental impacts. The devices for doing experiments in the future to capture vital parameters in the pond are very expensive, such as the DO sensor, NH_3 sensor, NO_2 sensor, and NO_3 sensor. Therefore, designing such devices with lower costs, equivalent accuracy, and reliable operation would be focused on future work.

In general, these plans will be beneficial and shorten the distance of applying high technology for aquaculture, particularly in developing countries with the ultimate goal of being sustainable cultivation, increasing the productivity and profits for farmers.

Appendices

Table A. 1 Specifications for selected PV module (ND-AH330H)

Parameter	Value
Standard test condition efficiency (%)	17
Temperature coefficient of open circuit (%/°C)	0.32
Voltage at point of maximum power (V)	37.8
Standard test condition temperature (°C)	25
Nominal operation cell temperature (°C)	45
Area of module (m^2)	1.94
Maximum power (W)	330

Table A. 2 Specifications for selected wind turbine system (DW61-500)

Parameter	Value	Refs
Cut-in speed (m/s)	2.5	
Rated speed (m/s)	10	
Cut-out speed (m/s)	25	
Mechanical efficiency (%)	100	
Electrical efficiency (%)	90	[126]
Power coefficient	0.4	
Air density (kg/m^3)	1.225	
Rated power (kW)	500	
Surface roughness length (m)	0.15	[127]

Table A. 3 Specifications for selected alkaline electrolyzer

Parameter	Value	Refs
The number of hydrogen molecules	2	
Average cell voltage (V)	1.9	[128]
Faraday number (C/mol)	96485	
Faradic efficiency (%)	95	[128]

Table A. 4 Specifications for selected fuel cell (PEM)

Parameter	Value	Refs
Coefficient of consumption curve (kg/Wh)	$4x10^{-6}$	[95]
Coefficient of consumption curve (kg/Wh)	$5x10^{-5}$	[95]
Output power at maximum efficiency (%)	20	[95]
Factor to consider the high consumption	1	[95]

Table A. 5 Specifications for selected hydrogen tank (compressed high-pressure)

Parameter	Value	Refs
Storage efficiency (%)	95	[116]

Table A. 6 Specifications for selected battery (NaS)

Parameter	Value	Refs
Charge control limit (%)	10	[129]
Battery efficiency (%)	90	[117]
Hourly self-discharge rate (%)	0	[117]

Table A. 7 Specifications for selected inverter (PVH-L2550)

Parameter	Value
Efficiency (%)	98

Table A. 8 Specifications for selected diesel generator

Parameter	Value	Refs
Intercept coefficient of fuel consumption curve (L/kWh)	0.08145	[97]
Slope of fuel consumption curve (L/kWh)	0.2461	[97]

Table A. 9 CO_2 emission factors

Parameter	Value	Refs
Emission factor from grid (g/kWh)	636	[130]
Emission factor from diesel fuel (g/kWh)	267	[131]

Table A. 10 Specifications for paddlewheel aerator

Parameter	Value
Aeration efficiency (kg/kWh)	1.68
Efficiency of electrical motor (%)	90

Bibliography

[1] F. A. O. U. Nations, "Global fish economy," in *Globefish Highlights - Issue 2/2019: A Quarterly Update on World Seafood Markets April 2019 Issue, with January–December 2018 Statistics*, 2nd ed. Rome, Italy: Food & Agriculture Org., 2019, pp. 11-13.

[2] F. A. O. U. Nations, *GLOBEFISH Highlights – Issue 1/2018: A quarterly update on world seafood markets*. FOOD & AGRICULTURE ORGN, 2018.

[3] G. Amagliani, G. Brandi, and G. F. Schiavano, "Incidence and role of Salmonella in seafood safety," *Food Research International,* vol. 45, no. 2, pp. 780-788, 2012.

[4] C. E. Boyd, E. Jory Darryl, G. W. Chamberlain, and A. Global Aquaculture, *Operating procedures for shrimp farming : global shrimp OP survey results and recommentations*. St. Louis, Missouri, USA: Global Aquaculture Alliance (in English), 2006.

[5] F. A. O. U. Nations, "Shrimp," in *Globefish Highlights - Issue 2/2019: A Quarterly Update on World Seafood Markets April 2019 Issue, with January–December 2018 Statistics*, 2nd ed. Rome, Italy: Food & Agriculture Org., 2019, pp. 14-18.

[6] O. M. Joffre, L. Klerkx, and T. N. Khoa, "Aquaculture innovation system analysis of transition to sustainable intensification in shrimp farming," *Agronomy for Sustainable Development,* vol. 38, no. 3, p. 34, 2018.

[7] N. Tho, N. Vromant, N. T. Hung, and L. Hens, "Soil salinity and sodicity in a shrimp farming coastal area of the Mekong Delta, Vietnam," *Environmental Geology,* vol. 54, no. 8, pp. 1739-1746, 2008.

[8] P. T. Anh, C. Kroeze, S. R. Bush, and A. P. Mol, "Water pollution by intensive brackish shrimp farming in south-east Vietnam: Causes and options for control," *Agricultural Water Management,* vol. 97, no. 6, pp. 872-882, 2010.

[9] C. E. Boyd, C. Tucker, A. McNevin, K. Bostick, and J. Clay, "Indicators of resource use efficiency and environmental performance in fish and crustacean aquaculture," *Reviews in Fisheries science,* vol. 15, no. 4, pp. 327-360, 2007.

[10] E. Peterson, "Prawn farm energy audits and five star ratings," *Aquaculture Asia,* vol. 7, no. 2, pp. 4-4, 2002.

[11] C. E. Boyd, "Pond water aeration systems," *Aquacultural engineering,* vol. 18, no. 1, pp. 9-40, 1998.

[12] S. Sombatjinda, N. Boonapatcharoen, M. Ruengjitchatchawalya, C. Wantawin, B. Withyachumnarnkul, and S. Techkarnjanaruk, "Dynamics of microbial communities in an earthen shrimp pond during the shrimp growing period," *Environment and natural resources research,* vol. 1, no. 1, p. 171, 2011.

[13] P. A. Sandifer and J. S. Hopkins, "Conceptual design of a sustainable pond-based shrimp culture system," *Aquacultural Engineering,* vol. 15, no. 1, pp. 41-52, 1996.

[14] R. R. E. Laboratory, *Design Manual: Fine Pore Aeration Systems*. US Environmental Protection Agency, Office of Research and Development …, 1989.

[15] S. Moulick, B. Mal, and S. Bandyopadhyay, "Prediction of aeration performance of paddle wheel aerators," *Aquacultural Engineering,* vol. 25, no. 4, pp. 217-237, 2002.

[16] J. M. Moore and C. E. Boyd, "Design of small paddle wheel aerators," *Aquacultural engineering,* vol. 11, no. 1, pp. 55-69, 1992.

[17] C. E. Boyd, "Water quality management and aeration in shrimp farming," 1989.
[18] C. Boyd, "Estimating mechanical aeration requirement in shrimp ponds from the oxygen demand of feed," *The Rising Tide, Proceedings of the Special Session on Sustainable Shrimp Farming,* pp. 230-34, 2009.
[19] C. E. Boyd, E. L. Torrans, and C. S. Tucker, "Dissolved oxygen and aeration in ictalurid catfish aquaculture," *Journal of the World Aquaculture Society,* vol. 49, no. 1, pp. 7-70, 2018.
[20] C. E. Boyd, E. Jory Darryl, G. W. Chamberlain, and A. Global Aquaculture, "Aerated pond management," in *Operating Procedures for Shrimp Farming: Global Shrimp OP Survey Results and Recommendations*, 1st ed. St. Louis, MO, USA: Global Aquaculture Alliance, 2006, pp. 68-75.
[21] E. L. Peterson, "Energy-efficiency manual for aquaculture pond aeration," 2003.
[22] D. Zhu, X. Cheng, D. J. Sample, and M. N. Yazdi, "Effect of intermittent aeration mode on nitrogen concentration in the water column and sediment pore water of aquaculture ponds," *journal of environmental sciences,* vol. 90, pp. 331-342, 2020.
[23] R. H. Hoagland, D. B. Rouse, D. Teichert-Coddington, and C. E. Boyd, "Evaluation of automated aeration control in shrimp ponds," *Journal of Applied Aquaculture,* vol. 11, no. 3, pp. 45-55, Sep 2001.
[24] W. Elmessery and S. Abdallah, "Intelligent dissolved oxygen control system for intensive carp system," *Journal of Agricultural Engineering and Biotechnology,* vol. 2, no. 4, p. 49, 2014.
[25] F. C. Cruz, K. Mahmudov, A. Marouchos, and A. Bilton, "A Feasibility Study on the Benefits of Feedback Aerator Control in Precision Aquaculture Applications for the Developing World," in *International Design Engineering Technical Conferences and Computers and Information in Engineering Conference*, 2019, vol. 59193: American Society of Mechanical Engineers, p. V02BT03A004.
[26] H. Deng, L. Peng, J. Zhang, C. Tang, H. Fang, and H. Liu, "An intelligent aerator algorithm inspired-by deep learning," *Mathematical biosciences and engineering: MBE,* vol. 16, no. 4, pp. 2990-3002, 2019.
[27] S. Thakre, L. Bhuyar, and S. Deshmukh, "Effect of different configurations of mechanical aerators on oxygen transfer and aeration efficiency with respect to power consumption," *International Journal of Aerospace and Mechanical Engineering,* vol. 2, no. 2, pp. 100-108, 2008.
[28] M. Adel, M. R. Shaalan, R. M. Kamal, and D. S. El Monayeri, "A comparative study of impeller aerators configurations," *Alexandria Engineering Journal,* vol. 58, no. 4, pp. 1431-1438, 2019.
[29] S. M. Roy1i, S. Moulick, C. K. Mukherjee, and B. C. Mal, "Effect of rotational speeds of paddle wheel aerator on aeration cost," 2015.
[30] S. M. Roy, S. Moulick, and B. C. Mal, "Design characteristics of spiral aerator," *Journal of the world aquaculture society,* vol. 48, no. 6, pp. 898-908, 2017.
[31] J. Marappan *et al.*, "Assessment of the new generation aeration systems efficiency and water current flow rate, its relation to the cost economics at varying salinities for Penaeus vannamei culture," *Aquaculture Research,* 2020.
[32] T. Itano *et al.*, "Water circulation induced by mechanical aerators in a rectangular vessel for shrimp aquaculture," *Aquacultural Engineering,* vol. 85, pp. 106-113, 2019.
[33] C. Zhang, B. Song, J. Shan, Q. Ni, F. Wu, and S. Wang, "Design and optimization of a new tube aeration device," *Aquaculture International,* pp. 1-15, 2020.

[34] F. Monforti-Ferrario and I. P. Pascua, *Energy use in the EU food sector: State of play and opportunities for improvement*. Publications Office, 2015.
[35] F. Hahn and R. Pérez, "Design and evaluation of a dissolved oxygen controller for solar powered fish tanks," *Current Journal of Applied Science and Technology,* pp. 173-188, 2015.
[36] P. E. Campana, L. Wästhage, W. Nookuea, Y. Tan, and J. Yan, "Optimization and assessment of floating and floating-tracking PV systems integrated in on- and off-grid hybrid energy systems," *solar energy,* vol. 177, pp. 782-795, 2019.
[37] C. Ioakeimidis, H. Polatidis, and D. Haralambopoulos, "Use of renewable energy in aquaculture: an energy audit case-study analysis," *Global NEST Journal,* vol. 15, no. 3, pp. 282-294, 2013.
[38] A. Mahmoud, T. N. Quang, E. Pavlov, and A. Bilton, "Development of a solar updraft aeration system for pond aquaculture in resource-constrained environments," in *2015 IEEE Global Humanitarian Technology Conference (GHTC)*, 2015: IEEE, pp. 306-313.
[39] K. Mahmudov, A. Mahmoud, S. Sur, F. C. Cruz, and A. M. Bilton, "Feasibility of a wind-powered aeration system for small-scale aquaculture in developing countries," *Energy for Sustainable Development,* vol. 51, pp. 40-49, 2019.
[40] C.-m. Lai and T.-h. Lin, "Technical assessment of the use of a small-scale wind power system to meet the demand for electricity in a land aquafarm in Taiwan," *Renewable Energy,* vol. 31, no. 6, pp. 877-892, 2006.
[41] W. Nookuea, P. E. Campana, and J. Yan, "Evaluation of solar PV and wind alternatives for self renewable energy supply: Case study of shrimp cultivation," *Energy Procedia,* vol. 88, pp. 462-469, 2016.
[42] M. Menicou and V. Vassiliou, "Prospective energy needs in Mediterranean offshore aquaculture: Renewable and sustainable energy solutions," *Renewable and Sustainable Energy Reviews,* vol. 14, no. 9, pp. 3084-3091, 2010.
[43] J. Ferreira, C. Saurel, J. L. e Silva, J. Nunes, and F. Vazquez, "Modelling of interactions between inshore and offshore aquaculture," *Aquaculture,* vol. 426, pp. 154-164, 2014.
[44] H. S. Das, C. W. Tan, and A. Yatim, "Fuel cell hybrid electric vehicles: A review on power conditioning units and topologies," *Renewable and Sustainable Energy Reviews,* vol. 76, pp. 268-291, 2017.
[45] D. M. Atia, F. H. Fahmy, N. M. Ahmed, and H. T. Dorrah, "A new control and design of PEM fuel cell powered air diffused aeration system," *TELKOMNIKA Indonesian Journal of Electrical Engineering,* vol. 10, no. 2, pp. 291-302, 2012.
[46] D. M. Atia, F. H. Fahmy, N. M. Ahmed, and H. T. Dorrah, "Design and Control of PEM Fuel Cell Diffused Aeration System using Artificial Intelligence Techniques," *International Journal of Electrical and Computer Engineering,* vol. 5, no. 9, pp. 1191-1198, 2011.
[47] Y. Shiratori *et al.*, "Biogas Power Generation with SOFC to Demonstrate Energy Circulation Suitable for Mekong Delta, Vietnam," *Fuel Cells,* vol. 19, no. 4, pp. 346-353, 2019.
[48] Y. Jianwei, S. Guolong, K. Cunjiang, and Y. Tianjun, "Oxygen blast furnace and combined cycle (OBF-CC)—an efficient iron-making and power generation process," *Energy,* vol. 28, no. 8, pp. 825-835, 2003.
[49] A. Macleod, "Economic use of electrolysed oxygen in rural or remote regions," *Energy Materials,* vol. 2, no. 1, pp. 1-4, 2007.
[50] T. N. Hai, T. Minh, T. Phu, and N. Phuong, "Shrimp industry in Vietnam," *Progress of shrimp and prawn aquaculture in the world. National Taiwan Ocean*

University, Keelung Taiwan, The Fisheries Society, Manila, Philippines, and Word Aquaculture Society, Louisiana, USA, pp. 181-204, 2016.
[51] N. T. Hien, "Statistic report - December 2017," 2017.
[52] A. Suzuki and V. H. Nam, "Better management practices and their outcomes in shrimp farming: evidence from small-scale shrimp farmers in Southern Vietnam," *Aquaculture International,* vol. 26, no. 2, pp. 469-486, 2018.
[53] A. W. Fast, "CHAPTER 14 - PENAEID GROWOUT SYSTEMS: AN OVERVIEW," in *Marine Shrimp Culture*, A. W. Fast and L. J. Lester Eds. Amsterdam: Elsevier, 1992, pp. 345-353.
[54] F. Apud, J. Primavera, and P. Torres, "Farming of prawns and shrimps extension manual no. 5," *Aquaculture Dept. SEAFDEC,* p. 67, 1983.
[55] T. Ahmad and C. E. Boyd, "Design and peroormance of paddle wheel aerators," *Aquacultural Engineering,* vol. 7, no. 1, pp. 39-62, 1988.
[56] A. W. Fast and J. E. Lannan, "CHAPTER 21 - POND DYNAMIC PROCESSES," in *Marine Shrimp Culture*, A. W. Fast and L. J. Lester Eds. Amsterdam: Elsevier, 1992, pp. 431-456.
[57] C. E. Boyd and A. W. Fast, "CHAPTER 23 - POND MONITORING AND MANAGEMENT," in *Marine Shrimp Culture*, A. W. Fast and L. J. Lester Eds. Amsterdam: Elsevier, 1992, pp. 497-513.
[58] F. Environmental, "Dissolved Oxygen: Fundamentals of Environmental Measurements," ed, 2013.
[59] J. E. Alleman and T. Prakasam, "Reflections on seven decades of activated sludge history," *Journal (Water Pollution Control Federation),* pp. 436-443, 1983.
[60] L. Vinatea, W. Muedas, and R. Arantes, "The impact of oxygen consumption by the shrimp Litopenaeus vannamei according to body weight, temperature, salinity and stocking density on pond aeration: a simulation," *Acta Scientiarum. Biological Sciences,* vol. 33, no. 2, pp. 125-132, 2011.
[61] W. Chunrong *et al.*, "Utilizing wind energy to develop aquaculture industry," 1994.
[62] A. W. Fast and C. E. Boyd, "CHAPTER 22 - WATER CIRCULATION, AERATION AND OTHER MANAGEMENT PRACTICES," in *Marine Shrimp Culture*, A. W. Fast and L. J. Lester Eds. Amsterdam: Elsevier, 1992, pp. 457-495.
[63] G. Rogers, "Aeration theory and its application to shrimp culture," *World Aquaculture Society,* pp. 211-219, 2009.
[64] C. E. Boyd and T. Ahmad, "Evaluation of aerators for channel catfish farming," 1987.
[65] J. Colt and B. Watten, "Applications of pure oxygen in fish culture," *Aquacultural Engineering,* vol. 7, no. 6, pp. 397-441, 1988.
[66] K. Q. Nguyen, "Alternatives to grid extension for rural electrification: Decentralized renewable energy technologies in Vietnam," *Energy Policy,* vol. 35, no. 4, pp. 2579-2589, 2007.
[67] J. Polo, A. Bernardos, S. Martínez, and C. F. Peruchena, "Maps of solar resource and potential in Vietnam," 2015.
[68] T. Le, "AN OVERVIEW OF THE RENEWABLE ENERGY POTENTIALS IN THE MEKONG RIVER DELTA, VIETNAM," *Gazi University Journal of Science,* pp. 70-79, 08/01 2016.
[69] A. Kies, B. Schyska, D. T. Viet, L. von Bremen, D. Heinemann, and S. Schramm, "Large-scale integration of renewable power sources into the Vietnamese power system," *Energy Procedia,* vol. 125, pp. 207-213, 2017.

[70] A. Ursua, L. M. Gandia, and P. Sanchis, "Hydrogen production from water electrolysis: current status and future trends," *Proceedings of the IEEE,* vol. 100, no. 2, pp. 410-426, 2011.

[71] D. Van Halem, H. Van der Laan, S. Heijman, J. Van Dijk, and G. Amy, "Assessing the sustainability of the silver-impregnated ceramic pot filter for low-cost household drinking water treatment," *Physics and Chemistry of the Earth, Parts A/B/C,* vol. 34, no. 1-2, pp. 36-42, 2009.

[72] K. Muroyama, K. Imai, Y. Oka, and J. i. Hayashi, "Mass transfer properties in a bubble column associated with micro-bubble dispersions," *Chemical Engineering Science,* vol. 100, pp. 464-473, 2013.

[73] L. Legrand, P. van Vugt, and R. van der Velde, "20% Reduction of CO2-Emissions with Power-to-Gas in WWTP," in *Proceedings of REHVA Annual Conference" Advanced HVAC and Natural Gas Technologies"*, 2015, pp. 250-253.

[74] S. Pascuzzi, A. S. Anifantis, I. Blanco, and G. Scarascia Mugnozza, "Electrolyzer performance analysis of an integrated hydrogen power system for greenhouse heating. A case study," *Sustainability,* vol. 8, no. 7, p. 629, 2016.

[75] Danmark and Energistyrelsen, "Overview of Vietnam energy sector," in *Vietnam Energy Outlook Report 2017*, 1st ed. Hanoi, Vietnam: Danish Energy Agency, 2018, pp. 11-50.

[76] F. Barbir, "PEM electrolysis for production of hydrogen from renewable energy sources," *Solar energy,* vol. 78, no. 5, pp. 661-669, 2005.

[77] F. Barbir, M. Lillis, F. Mitlitsky, and T. Molter, "Regenerative fuel cell applications and design options," in *Proceedings of 14th World Hydrogen Energy Conference, Montreal, Canada. As referenced in Ref*, 2002, vol. 35.

[78] R. K. Gelda, M. T. Auer, S. W. Effler, S. C. Chapra, and M. L. Storey, "Determination of reaeration coefficients: whole-lake approach," *Journal of Environmental Engineering,* vol. 122, no. 4, pp. 269-275, 1996.

[79] J. Crusius and R. Wanninkhof, "Gas transfer velocities measured at low wind speed over a lake," *Limnology and Oceanography,* vol. 48, no. 3, pp. 1010-1017, 2003.

[80] Z. Xu and Y. J. Xu, "A deterministic model for predicting hourly dissolved oxygen change: development and application to a shallow eutrophic lake," *Water,* vol. 8, no. 2, p. 41, 2016.

[81] A. W. Fast and C. E. Boyd, "Water circulation, aeration and other management practices," *Developments in aquaculture and fisheries science,* vol. 23, pp. 457-495, 1992.

[82] C. Bett and L. Vinatea, "Combined effect of body weight, temperature and salinity on shrimp Litopenaeus vannamei oxygen consumption rate," *Brazilian Journal of Oceanography,* vol. 57, no. 4, pp. 305-314, 2009.

[83] J. Ivy, "Summary of electrolytic hydrogen production: milestone completion report," National Renewable Energy Lab., Golden, CO (US), 2004.

[84] C.-H. Li, X.-J. Zhu, G.-Y. Cao, S. Sui, and M.-R. Hu, "Dynamic modeling and sizing optimization of stand-alone photovoltaic power systems using hybrid energy storage technology," *Renewable energy,* vol. 34, no. 3, pp. 815-826, 2009.

[85] I. Blanco, S. Pascuzzi, A. S. Anifantis, and G. Scarascia-Mugnozza, "Study of a pilot photovoltaic-electrolyser-fuel cell power system for a geothermal heat pump heated greenhouse and evaluation of the electrolyser efficiency and operational mode," *Journal of Agricultural Engineering,* vol. 45, no. 3, pp. 111-118, 2014.

[86] P. Choi, D. G. Bessarabov, and R. Datta, "A simple model for solid polymer electrolyte (SPE) water electrolysis," *Solid State Ionics,* vol. 175, no. 1-4, pp. 535-539, 2004.
[87] C. E. Boyd and C. S. Tucker, "Aeration," in *Pond Aquaculture Water Quality Management*. Boston, MA: Springer US, 1998, pp. 306-353.
[88] A. Kumar, S. Moulick, and B. C. Mal, "Selection of aerators for intensive aquacultural pond," *Aquacultural engineering,* vol. 56, pp. 71-78, 2013.
[89] "Design of Photovoltaic Systems," in *Solar Engineering of Thermal Processes, Photovoltaics and Wind*, pp. 760-788.
[90] "Available Solar Radiation," in *Solar Engineering of Thermal Processes, Photovoltaics and Wind*, pp. 45-140.
[91] R. Chedid, H. Akiki, and S. Rahman, "A decision support technique for the design of hybrid solar-wind power systems," *IEEE transactions on Energy conversion,* vol. 13, no. 1, pp. 76-83, 1998.
[92] A. Kanase-Patil, R. Saini, and M. Sharma, "Sizing of integrated renewable energy system based on load profiles and reliability index for the state of Uttarakhand in India," *Renewable Energy,* vol. 36, no. 11, pp. 2809-2821, 2011.
[93] "Wind Characteristics and Resources," in *Wind Energy Explained*, pp. 23-89.
[94] A. Askarzadeh, "A discrete chaotic harmony search-based simulated annealing algorithm for optimum design of PV/wind hybrid system," *Solar Energy,* vol. 97, pp. 93-101, 2013.
[95] R. Dufo-Lopez and J. L. Bernal-Agustín, "Multi-objective design of PV–wind–diesel–hydrogen–battery systems," *Renewable energy,* vol. 33, no. 12, pp. 2559-2572, 2008.
[96] A. K. Kaviani, G. Riahy, and S. M. Kouhsari, "Optimal design of a reliable hydrogen-based stand-alone wind/PV generating system, considering component outages," *Renewable energy,* vol. 34, no. 11, pp. 2380-2390, 2009.
[97] M. S. Ismail, M. Moghavvemi, and T. Mahlia, "Techno-economic analysis of an optimized photovoltaic and diesel generator hybrid power system for remote houses in a tropical climate," *Energy conversion and management,* vol. 69, pp. 163-173, 2013.
[98] M. Campbell, P. Aschenbrenner, J. Blunden, E. Smeloff, and S. Wright, "The drivers of the levelized cost of electricity for utility-scale photovoltaics," *White Paper: SunPower Corporation,* 2008.
[99] S. Mathew, "Economics of wind energy," in *Wind Energy: Fundamentals, Resource Analysis and Economics*. Berlin, Heidelberg: Springer Berlin Heidelberg, 2006, pp. 209-236.
[100] B. Ai, H. Yang, H. Shen, and X. Liao, "Computer-aided design of PV/wind hybrid system," *Renewable energy,* vol. 28, no. 10, pp. 1491-1512, 2003.
[101] S. Chen *et al.*, "The potential of photovoltaics to power the belt and road initiative," *Joule,* vol. 3, no. 8, pp. 1895-1912, 2019.
[102] M. Dakkak and A. Hasan, "A charge controller based on microcontroller in stand-alone photovoltaic systems," *Energy Procedia,* vol. 19, pp. 87-90, 2012.
[103] Y. E. A. Eldahab, N. H. Saad, and A. Zekry, "Enhancing the design of battery charging controllers for photovoltaic systems," *Renewable and Sustainable Energy Reviews,* vol. 58, pp. 646-655, 2016.
[104] K. Deb, "Elitist multi-objective evolutionary algorithms," in *Multi-Objective Optimization Using Evolutionary Algorithms*: Wiley, 2009, pp. 239-288.
[105] Y. Katsigiannis, P. Georgilakis, and E. Karapidakis, "Multiobjective genetic algorithm solution to the optimum economic and environmental performance

problem of small autonomous hybrid power systems with renewables," *IET Renewable Power Generation,* vol. 4, no. 5, pp. 404-419, 2010.
[106] D. F. Pires, C. H. Antunes, and A. G. Martins, "NSGA-II with local search for a multi-objective reactive power compensation problem," *International Journal of Electrical Power & Energy Systems,* vol. 43, no. 1, pp. 313-324, 2012.
[107] R. Dufo-Lopez, I. R. Cristobal-Monreal, and J. M. Yusta, "Stochastic-heuristic methodology for the optimisation of components and control variables of PV-wind-diesel-battery stand-alone systems," *Renewable Energy,* vol. 99, pp. 919-935, 2016.
[108] P. Vithayasrichareon and I. F. MacGill, "A Monte Carlo based decision-support tool for assessing generation portfolios in future carbon constrained electricity industries," *Energy policy,* vol. 41, pp. 374-392, 2012.
[109] M. Perninge and C. Hamon, "A stochastic optimal power flow problem with stability constraints—Part II: The optimization problem," *IEEE Transactions on Power Systems,* vol. 28, no. 2, pp. 1849-1857, 2012.
[110] J. Polo *et al.*, "Solar resources and power potential mapping in Vietnam using satellite-derived and GIS-based information," *Energy Conversion and Management,* vol. 98, pp. 348-358, 2015.
[111] S. Joost and A. Eric, "Wind Energy Potential Vietnam," Netherlands Enterprise Agency, The Netherlands, RVO-015-1901-RP-INT, 2018.
[112] C. E. Boyd and C. S. Tucker, "Ecology of aquaculture ponds," in *Pond aquaculture water quality management*: Springer, 1998, pp. 8-86.
[113] N. Q. Khanh, "Analysis of future generation capacity scenarios for Vietnam," in "Green Innovation and Development Centre (GreenID), Vietnam," GreenID., Hanoi, Vietnam, Oct 2017.
[114] A. Buttler and H. Spliethoff, "Current status of water electrolysis for energy storage, grid balancing and sector coupling via power-to-gas and power-to-liquids: A review," *Renewable and Sustainable Energy Reviews,* vol. 82, pp. 2440-2454, 2018.
[115] S. M. Hakimi, A. Hasankhani, M. Shafie-khah, and J. P. Catalão, "Optimal sizing and siting of smart microgrid components under high renewables penetration considering demand response," *IET Renewable Power Generation,* vol. 13, no. 10, pp. 1809-1822, 2019.
[116] Z. Huang *et al.*, "Modeling and multi-objective optimization of a stand-alone PV-hydrogen-retired EV battery hybrid energy system," *Energy conversion and management,* vol. 181, pp. 80-92, 2019.
[117] X. Luo, J. Wang, M. Dooner, and J. Clarke, "Overview of current development in electrical energy storage technologies and the application potential in power system operation," *Applied energy,* vol. 137, pp. 511-536, 2015.
[118] R. Fu, D. J. Feldman, and R. M. Margolis, "US solar photovoltaic system cost benchmark: Q1 2018," National Renewable Energy Lab.(NREL), Golden, CO (United States), 2018.
[119] Z. Movahediyan and A. Askarzadeh, "Multi-objective optimization framework of a photovoltaic-diesel generator hybrid energy system considering operating reserve," *Sustainable cities and society,* vol. 41, pp. 1-12, 2018.
[120] D. E. Agency, "Vietnam Energy Outlook Report 2017," 2017.
[121] J. Armijo and C. Philibert, "Flexible production of green hydrogen and ammonia from variable solar and wind energy: Case study of Chile and Argentina," *International Journal of Hydrogen Energy,* vol. 45, no. 3, pp. 1541-1558, 2020.

[122] S. Mandal, B. K. Das, and N. Hoque, "Optimum sizing of a stand-alone hybrid energy system for rural electrification in Bangladesh," *Journal of Cleaner Production,* vol. 200, pp. 12-27, 2018.
[123] S. Singh, M. Singh, and S. C. Kaushik, "Feasibility study of an islanded microgrid in rural area consisting of PV, wind, biomass and battery energy storage system," *Energy Conversion and Management,* vol. 128, pp. 178-190, 2016.
[124] T. C. Nguyen and A. T. Chuc, "Green finance in Viet Nam: Barriers and solutions," ADBI Working Paper Series, 2018.
[125] G. Merei, C. Berger, and D. U. Sauer, "Optimization of an off-grid hybrid PV–Wind–Diesel system with different battery technologies using genetic algorithm," *Solar Energy,* vol. 97, pp. 460-473, 2013.
[126] H. Li and Z. Chen, "Overview of different wind generator systems and their comparisons," *IET Renewable Power Generation,* vol. 2, no. 2, pp. 123-138, 2008.
[127] A. Truepower, "Wind Resource Atlas of Viet Nam," 2011.
[128] J. Wanjiku, M. Khan, P. Barendse, and A. Sebitosi, "Analytical sizing of an electrolyser for a small scale wind electrolysis plant," in *2010 IEEE International Energy Conference*, 2010: IEEE, pp. 10-15.
[129] E. Banguero, A. Correcher, Á. Pérez-Navarro, F. Morant, and A. Aristizabal, "A review on battery charging and discharging control strategies: Application to renewable energy systems," *Energies,* vol. 11, no. 4, p. 1021, 2018.
[130] S. Rieseberg and C. Wörlen, *Situation Analysis of the Vietnamese Electricity Sector*. 2017.
[131] Asian Development Bank, "General methodology," in *Guidelines for estimating greenhouse gas emissions of Asian development bank projects: additional guidance for clean energy projects*, 1st ed. Manila, Philippines: Asian Development Bank, 2017, pp. 2-7.

Research Achievements

Oral Presentations

1. "A sustainable energy model for shrimp farms in the mekong delta." Technologies and Materials for Renewable Energy, Environment and Sustainability, TMREES18, Athen, Greece, 09/2018.
2. "A Renewable Energy Model for Shrimp Farms." 第 35 回エネルギーシステム・経済・環境コンファレンス.

Publications

1. Tien, Nguyen Nhut, Ryuji Matsuhashi, and Vo Tran Thi Bich Chau. "A sustainable energy model for shrimp farms in the mekong delta." Energy Procedia 157 (2019): 926-938.
2. Nguyen, Nhut Tien, and Ryuji Matsuhashi. "An Optimal Design on Sustainable Energy Systems for Shrimp Farms." IEEE Access 7 (2019): 165543-165558.
3. Nguyen, Nhut Tien, and Ryuji Matsuhashi. "A Design on Sustainable Hybrid Energy Systems by Multiobjective Optimization for Aquaculture Industry." Renewable Energy (Under revision).